Authors Reply to Anonymous Referee #1

This paper show low ozone and water vapor near the tropopause at Kunming, China, from Balloonsonde measurements. Multiple data sets support these results, e.g., Feng Yun-2D, FengYun-2G, Aura Microwave Limb Sounder (MLS) satellite data. The observed low ozone and low water vapor are attributed to transport of boundary layer air parcels originated from deep convection region associated with tropical cyclones in the western Pacific. Then dehydration of air parcels happens while passing through the coldest temperature region in the UTLS. Dehydration is also linked to convective clouds associated with the cyclone in the pacific. The results also highlight that vertical transport is faster and stronger in ERA5 than ERA-Interim. This situation was observed in two cases 1-8 August 2009 and 10th August 2015.

The Authors have presented the results with sufficient pieces of evidence and justifications. The manuscript should be published in the ACP after the revision.

I have the following few suggestions which authors may consider to include during revision.

Reply: The authors appreciate the anonymous referee #1 for your constructive and meaningful comments which are very helpful for our manuscript. Please see below our responses point by point (*referees' comments in blue with italics font* and our response in black). Further, the revised manuscript is added highlighting in colour any changes compared to the ACPD version.

In the years 2009 and 2015, there was El Niño in the pacific. Don't you think that vertical transport of air parcels will be influenced by warming at the onset phase of El Niño?

Reply: The long term ozone trend in the tropical stratosphere (17–21 km) is primarily linked to the QBO and ENSO (Randel and Thompson, 2011). ENSO variability in ozone is about 10% relative to local background levels. The ozone change is linked to enhanced zonal mean tropical stratospheric upwelling in ENSO warm events (Randel et al., 2009). We check the oceanic El Niño index from the webpage https://ggweather.com/enso/oni.htm . The 3-month (JJA) mean index is 0.5 in 2009 and 1.8 in 2015, respectively. There is a very strong El Niño in 2015. The ozone negative variability on 8 August 2009 and 2015 are about 60%. Ozone profiles without influence of typhoon in August of 2009 and 2015 show small variability (Figs. 2b and 9b in the revised manuscript). In 2013, the 3-month mean Oceanic Niño index value is -0.4. Li et al. (2017) show three tropical cyclones have uplifted the marine boundary air with low ozone to the tropical tropopause layer in August 2013. The ozone vertical transport within several days is strongly associated with the intense typhoon case. El Niño has in general the potential to impact vertical upward transport in the Pacific, however, the contribution to strong uplift within a single typhoon is to be assumed to be small. Further it is hard to differentiate between the impact of El Nino and tropical cyclones on vertical upward transport of air masses.

Linkages of dehydration of air mass with convective clouds in the Pacific associated with the cyclone and passage through coldest temperature region are not clear. It should be stated clearly in the discussion section and elsewhere.

Reply: We rewrite the sentence in the conclusions from "...Our case study for the summer season is consistent with this low temperature picture, with lowest temperatures also occurring over the western Pacific and at the southeastern edge of the ASM, however, further north compared to winter condition." to "...Our case studies show that the low temperature ($<$190 K) at the outflow of deep convective clouds associated with tropical cyclones causes freeze-drying in the tropopause layer during the summer season at the southeastern edge of the ASM. This result is consistent with results of Holton and Gettelman (2001) demonstrating that the low temperature picture in winter, with lowest temperatures also occurring over the western Pacific, and further northward of the ASM in contrast to winter conditions. "

It is excepted that the marine boundary layer containing low ozone and high water vapor may get dehydrated near the cold tropopause. Authors have cited several studies reporting poor ozone air arriving near the tropopause from the tropical marine boundary layer, and there is cold trap dehydration near the TTL (page 2 Lines 2-50). What are the new results?

Reply: The balloon-borne campaign over the Tibetan Plateau within the ASM anticyclone captures the low ozone and low water vapour at the same time. However, low ozone and high water vapour mixing ratios are common features in the ASM anticyclone as mentioned by referee#1. This is different to our observation where the impact of tropical cyclones on ozone and water vapour measurements is highlighted. Further, dehydration processes in the western Pacific discussed in the literature mainly took place during winter time. We added some more detailed explanations in abstract and conclusion.

Authors should highlight the implications of low ozone and low water vapor in the abstract and conclusions.

Reply: We added this sentence "Our findings show that the interplay between the ASM anticyclone and tropical cyclones have a significant impact on the chemical composition of the UTLS during summer." in abstract.
In conclusions, we added the following sentence "The interplay between tropical cyclones and the ASM anticyclone has the potential to impact the long term trends of ozone, water vapour, and even optically thin cirrus near the tropopause, particularly under climate change conditions, when the occurrence of tropical cyclones is expected to be more frequently."

Do you see low ozone and low water vapor values during the passage of cyclone, and low value disappears after that? Daily plots from 7–13 August 2009 and 3–18 August 2015 will be helpful.

Reply: Fig. 11a (in the revised manuscript) shows the ozone profiles measured by MLS satellite before, during, and after typhoon Soudelor passing through the Naha station. Ozone is low during typhoon period and quickly return to a normal value during the post-typhoon period. Balloons usually were launched in Naha once per week in summer. The last balloon profile maybe also get impact from another tropical cyclone over the western Pacific. (Daily) Variations of ozone and water vapour for 7–13 August 2009 and 3–18 August 2015 in Kunming are also shown in Fig. 1 (in this reply). Air parcels uplifted by a typhoon in the western Pacific need several days to be transported to Kunming (see Fig. 3 in the revised manuscript). The balloon campaign in Kunming usually launched balloons according to the local weather conditions. Heavy rain and thick clouds are bad conditions for the CFH (used to detect water vapour) and Cobald (used to detect cirrus and aerosol) measurements. Therefore, not for every day from 7–13 August 2009 and 3–18 August 2015 ozone and water vapour measurements are available. Instead, we show all ozone and water vapour profiles in Figs. 2 and 9 in the revised manuscript and highlight those profiles that are impacted by tropical cyclones.

Dehydration and ice formation can be shown in a figure from ERA5 and ERA-Interim to support the results.

Reply: Figure 2 show cloud ice water content and specific humidity from ERA-Interim and ERA5 in 2015. The detailed microphysical process associated with the cirrus at 15–20 km is difficult to reproduce in model simulation.

The authors should show a vertical profile-plot showing the difference between ozone on 8 August 2009 and daily climatological mean. A similar plot for water vapor will be useful. Also, similar plots for ozone and water vapor on 10 August 2015 should be shown in supplementary figures. It will help to quantify the decrease in ozone and water vapor at different altitudes on the respective days.

Reply: We added the following figures to the appendix of the revised manuscript.

Do you have observations that show low ozone and water vapor outside the cyclone days? Is it a regular feature near the TTL over China during August? Or is there stronger dehydration during cyclone days due to clouds (cumulonimbus) reaching the tropopause?

Reply: The authors check all of balloon-borne data in summer since 2009. There is no observation data outside of the cyclones, with low ozone and low water vapor at the same time. But there are few profiles with low water vapour mixing ratios. The reason for investigating low water vapour is ongoing much research.

Page 11 L 212–215: These statements are confusing. What is the reason for the dehydration of air parcel? Is it related to the deep convective clouds or due to the passage of air parcels through cirrus clouds?

Reply: According to the observation and model results, we think that the low water vapour is linked to the low temperature region which is associated with the outflow of deep convection. During the cirrus clouds are formed, air masses will be dehydrated.

One can use brightness temperature and optical thickness, both, to determine the presence of convective cloud or cirrus cloud. The method adopted for identification of convective cloud should be mentioned in section 3.1.1.

Reply: Thanks for this useful comment. We added the following comment "The CTT from FY-2G (105° E) employs single-

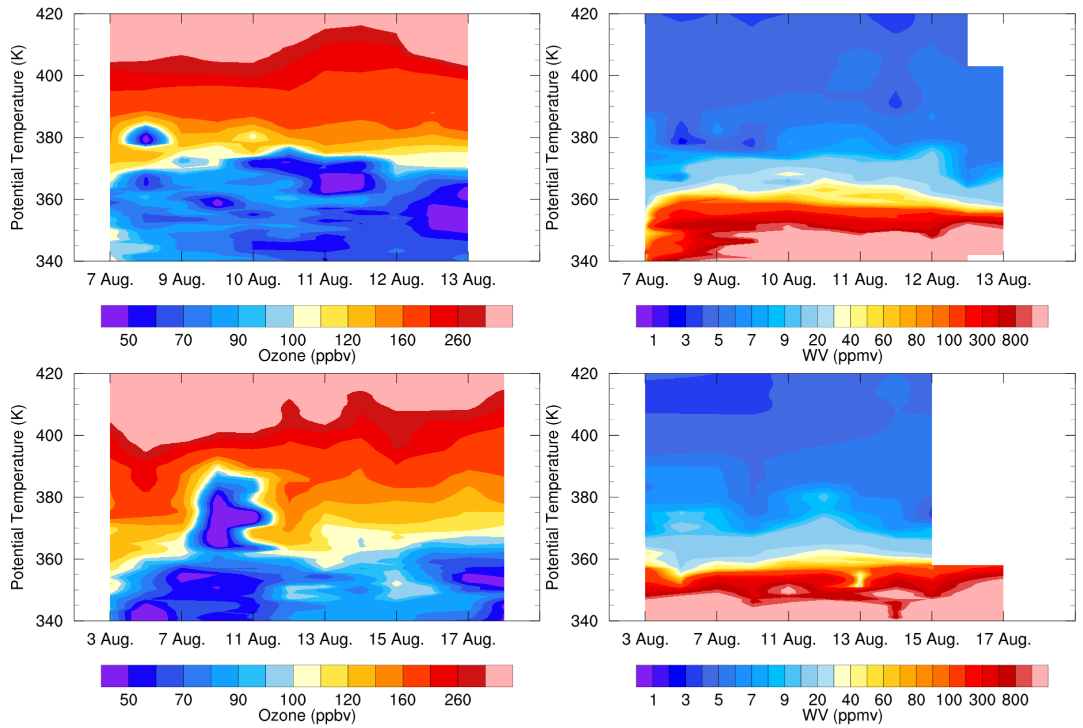

Figure 1. The variability of ozone and water vapour in August 2009 (top) and 2015 (bottom) deduced from balloon measurements in Kunming.

channel infrared (11μm) window area retrieval (**?**). Cloud radiating temperature is assumed to be $B(T) = (1-\varepsilon)B(T_{cs}) + \varepsilon B(T_c)$.

Where B is the Planck function. ε is the effective emissivity (**?**). CTT is computed with the cloud-top emissivity parameter (ε_t). For thick clouds, $\varepsilon_t = \varepsilon$.
For thin clouds, ε_t depends on T_c,
if T_c<245 K then $\varepsilon_t = (-0.00914 T_c + 2.966)\varepsilon$,
if T_c>280 K then $\varepsilon_t = (0.00753 T_c + 1.12)\varepsilon$.
The cloud-top temperature is
$T_t = B^{-1}\{[B(T) - (1-\varepsilon_t)B(T_{cs})] \vee \varepsilon_t\}$.

TBB>295 K in Fig. 7 is blackbody temperature, CTT>295 K in white for Fig. 14 means clear sky. To be consistent, we used FY-2G TBB instead of the CTT in the revised manuscript.".

Figure-1 shows geopotential height at 150 hPa on 4, 5, and 6 August 2009. Why not during all the days from 4–8 August 2009?
Reply: We added the geopotential height at 150 hPa on 7 and 8 August 2009 to Fig. 1.

Page 5–6: The outflow of deep convection is stronger on 6 August 2009 while the vertical profile of ozone and water vapor shows a low amount on 8 August 2009, Why?
Reply: Sure, the convective outflow is strongest on 6 August around Naha over the western Pacific. The transport of these air masses from Naha to Kunming over the Tibetan Plateau needs 2 days, therefore the profiles of water vapour and ozone in Kunming have low values on 8 August 2009.

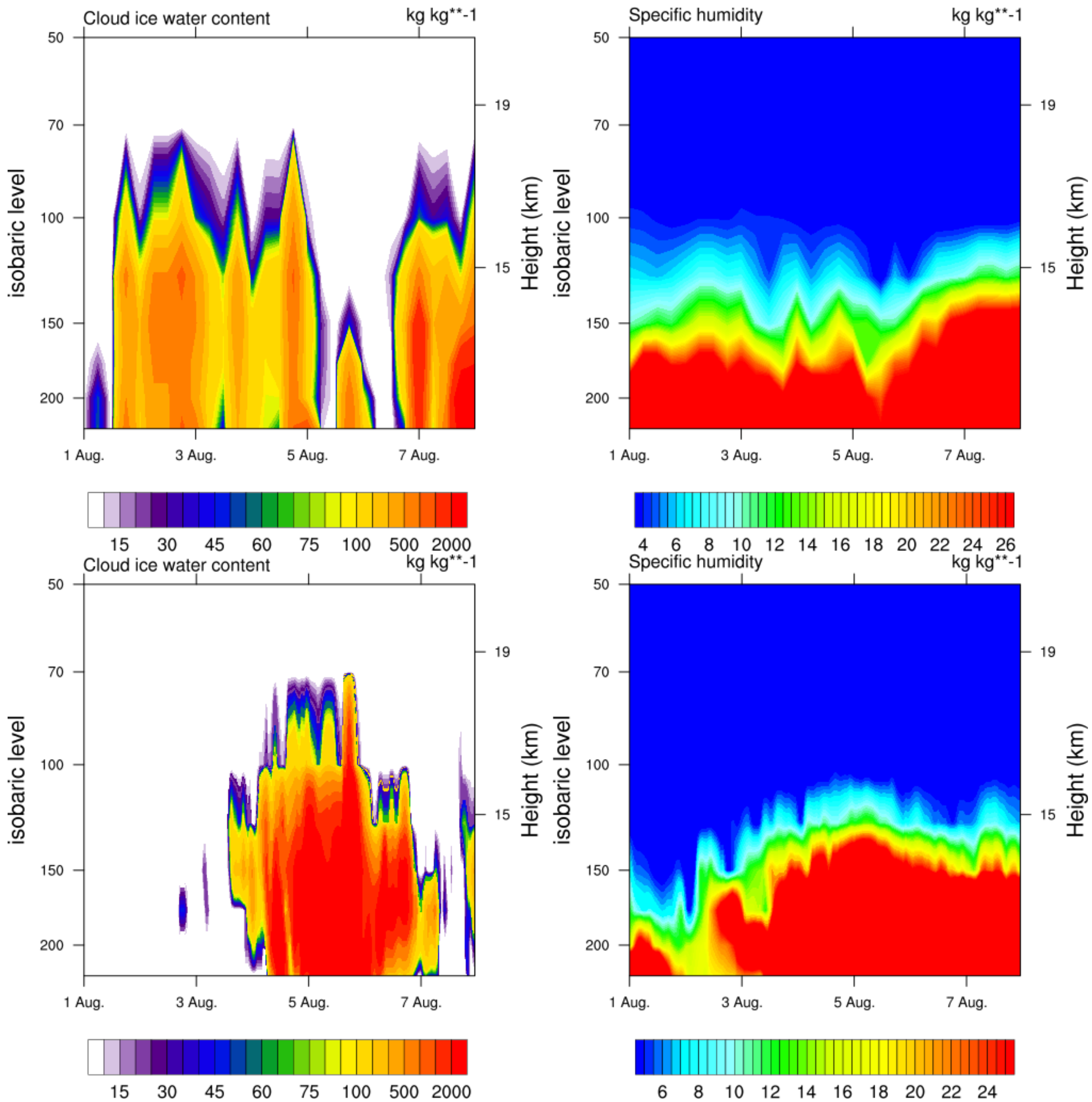

Figure 2. Daily variability of cloud ice water content (10^{-8} kg kg^{-1}) and specific humidity (10^{-6} kg kg^{-1}) from ERA-Interim (top) and ERA5 (bottom) reanalysis data in 2015.

Profiles of ozone show minimum ozone at a different height on 4th and 8 August 2009. Is it due to the distance of a cyclone from the observational site?

Reply: "Naha station is located approximately 2500 km east of Kunming, and these two sites are nearly on the same zonal line". The slow-scale upwelling at the top of the ASM (e.g. Vogel et al. (2019)) will uplift these air masses when moving from Naha to Kunming within 4 days.

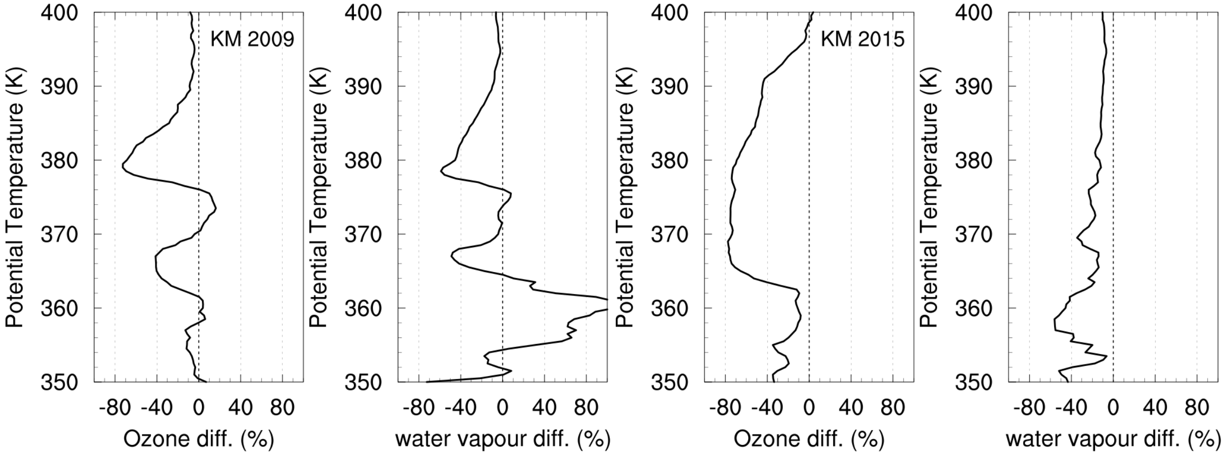

Figure 3. Ozone and water vapour relative difference on 8 August 2009 (left) and 10 August 2015 (right) to climatological mean value for August 2009 and 2015.

Page 12 Case 2: 10 August.
On 3 August 2015, intensity typhoon Soudelor reached Category 5. The authors should state the reason for showing analysis on 10 August 2015 when the typhoon was degraded to depression. Balloon measurements are available from 3 to 18 August 2015 (Page 3, L74). The authors should present a case for any day during 2–3 August 2015.

Reply: We show all ozone profiles in Kunming in August 2015 in Fig. 9b. The air masses in the UTLS over Kunming on 2–3 August 2015, moved backward in Naha will be in July, when tropical cyclone Soudelor are over the center Pacific, far away from Naha. In general, in situ ozone and water vapour measurements in the region of the Asian monsoon are sparse, therefore it is not often that the impact of a tropical cyclone is observed in a single measured ozone and water vapour profile.

Page 7, L 147, and Page 13L 246: If authors want to show vertical profiles which has no influence of cyclone, then profiles should be presented for the days before the formation of cyclone in the Pacific. Profiles on 4 August 2009 and 5 August 2015 are influenced by the cyclonic winds since on these days Morakot, and Soudelor cyclones were passing through the Pacific. If authors want to show the influence of cyclones, then profiles should be shown on the same days at Naha and Kunming. Is there any reason for choosing different days? If so, please clarify.

Reply: The profiles on 8 August 2009 and on 10 August 2015 over Kunming were influenced by tropical cyclones. Naha station is located approximately 2500 km east of Kunming, and these two sites are nearly on the same zonal line. According to the backward trajectory calculations (top panel of Fig. 5 and Fig. 12 in the revised manuscript), the same air masses in the upper troposphere and lower stratosphere in Naha should be influenced by cyclones 4–5 days before the air massed reach in Kunming. That is why we select the profiles on 4 August 2009 and 5 August 2015 in Naha. Balloons usually were launched in Naha once per week in summer. The last balloon profile maybe also get impact from another tropical cyclone. About this topic, another paper is in preparation that focus on the frequency and intensity of typhoon impact on the UTLS ozone in the western Pacific. We calculate the monthly mean ozone profiles (the grey profiles in Fig. 4a in the revised manuscript) instead of using the profile on measured a few days before the formation of cyclones Morakot and Soudelor over the Pacific.

ASM anticyclone is associated with a large amount of water vapor and low ozone. However, authors want to show that deep convective clouds associated with cyclone, which reaches near the tropopause (cold cloud tops), cause freeze-drying at the outflow of ice clouds. It should be made clear in the abstract and conclusions.

Reply: We revise the first sentence in abstract from "Low ozone and low water vapour values near the tropopause over Kunming, China were observed using balloon-borne measurements ..." to " Low ozone and high water vapour mixing ratios are common features in the Asian summer monsoon (ASM) anticyclone, however, low ozone and low water vapour values near

the tropopause over Kunming, China were observed within the ASM using balloon-borne measurements...".
The following sentences in conclusions are rewrite from "Our case study for the summer season is consistent with this low temperature picture, with lowest temperatures also occurring over the western Pacific and at the southeastern edge of the ASM, however, further north compared to winter condition." to "Our case studies show that the low temperature ($<$190 K) at the outflow of deep convective clouds associated with tropical cyclones causes freeze-drying in the tropopause layer during the summer season at the southeastern edge of the ASM. This result is consistent with results of Holton and Gettelman (2001) demonstrating that the low temperatures in winter, with the lowest temperatures occurring over the western Pacific, and causing freeze-drying in the winter tropopause layer. "

Figures: fonts of X-axis and Y-axis in all the figures should be bigger and bold.
Reply: Done for all the figures

References

Holton, J. R. and Gettelman, A.: Horizontal transport and the dehydration of the stratosphere, Geophys. Res. Lett., 28, 2799–2802, 2001.

Li, D., Vogel, B., Bian, J., Müller, R., Pan, L. L., Günther, G., Bai, Z., Li, Q., Zhang, J., Fan, Q., and Vömel, H.: Impact of typhoons on the composition of the upper troposphere within the Asian summer monsoon anticyclone: the SWOP campaign in Lhasa 2013, Atmos. Chem. Phys., 17, 4657–4672, https://doi.org/10.5194/acp-17-4657-2017, 2017.

Randel, W. J. and Thompson, A. M.: Interannual variability and trends in tropical ozone derived from SAGE II satellite data and SHADOZ ozonesondes, J. Geophys. Res., 116, D07303, https://doi.org/10.1029/2010JD015195, 2011.

Randel, W. J., Garcia, R. R., Calvo, N., and Marsh, D.: ENSO influence on zonal mean temperature and ozone in the tropical lower stratosphere, Geophys. Res. Lett., 36, L15822, https://doi.org/10.1029/2009GL039343, 2009.

Vogel, B., Müller, R., Günther, G., Spang, R., Hanumanthu, S., Li, D., Riese, M., and Stiller, G. P.: Lagrangian simulations of the transport of young air masses to the top of the Asian monsoon anticyclone and into the tropical pipe, Atmos. Chem. Phys., 19, 6007–6034, https://doi.org/10.5194/acp-2018-724, 2019.

Authors Reply to Anonymous Referee #2

This study presents low ozone and low water vapor layers observed in the tropopause layer over Kunming, southern China and discusses them from the perspective of air mass transport and dehydration. The balloon-borne observation results are unique and interesting. The analysis method combining satellite measurement data with trajectories driven by state-of-the-art reanalysis data is adequate and persuasive. The results are impressively presented and it seems to be fascinating for wide range of readers, even though the study is based only on two case studies. In my view, the paper should be published in ACP after minor revision. Some specific comments and suggestions are listed below, they are all minor.

Reply: The authors appreciate the anonymous referee #2 for these useful comments which were very helpful to the revised manuscript. Please see below our responses point by point (*referees' comments in blue with italics font* and our response in black). Further, the revised manuscript is added highlighting in colour any changes compared to the ACPD version.

Specific comments:

-Line 104–106: What is definitional or calculational difference between TBB and CTT? How about making a brief explanation of the two, here. Further, are the coloring somewhat different between Figs. 7 and 14? Region where >295 K is coloured in deep red for Fig. 7, but in white for Fig. 14?

Reply: The CTT from FY-2G (105° E) employs single-channel infrared (11μm) window area retrieval (Wang et al., 2018). Cloud radiating temperature is assumed to be $B(T) = (1-\varepsilon)B(T_{cs}) + \varepsilon B(T_c)$.

Where B is the Planck function. ε is the effective emissivity (Minnis et al., 1995). CTT is computed with the cloud-top emissivity parameter (ε_t). For thick clouds, $\varepsilon_t = \varepsilon$.

For thin clouds, ε_t depends on T_c,

if T_c<245 K then $\varepsilon_t = (-0.00914T_c + 2.966)\varepsilon$,

if T_c>280 K then $\varepsilon_t = (0.00753T_c + 1.12)\varepsilon$.

The cloud-top temperature is

$T_t = B^{-1}\{[B(T) - (1-\varepsilon_t)B(T_{cs})] \vee \varepsilon_t\}$.

TBB>295 K in Fig. 7 is blackbody temperature, CTT>295 K in white for Fig. 14 means clear sky. To be consistent, we used FY-2G TBB instead of the CTT in the revised manuscript.

-Section 3.1: How about adding the definition or citation for "lapse rate tropopause."

Reply: We rewrite this sentence from "The lapse rate tropopause potential temperature..." to "The World Meteorological Organization (WMO) tropopause potential temperature..." and citation "WMO1957".

- Line 204–206: The authors describe "Three days later, the mean water vapour mixing ratio of the same air parcels are about 3 ppmv, marked with red dot (right-hand side). The minimum SMR observed by CFH is approximate 2.7 ppmv in Kunming on 8 August," From this statement, I expect that the supersaturation had been observed because the water vapor mixing ratio is higher than the SMR. However, the RHiFP shown in Figure 4 is lower than 100% through the whole altitude. Is the "SMR" in line 205 a mistake of "water vapor mixing ratio"?

Reply: Thanks for finding this mistake. The authors corrected this statement from "...minimum SMR observed by CFH..." to "...minimum water vapor mixing ratio observed by CFH..."

- Line 209–211: I feel the descriptions are a little sudden. How about writing a little more particularly about what you are assuming and what you are comparing? For example, how about adding a statement, such as "If we assume that the air mass retains water vapor mixing ratio when it had been observed by the CFH," at the beginning of the sentence "air parcels have experienced supersaturation (RHi up to 180%) over ..."

Reply: Thanks for the advice, we added this statement in the revised manuscript.

In addition, the following is just a suggestion, but if the Lagrangian minimum SMR ($SMRmin_i$) that the each trajectory (trj_i) has experienced after the final convective encountering (latest $Tbb < T_{trj}$) is estimated, and the average SMRmin of all trajectories is calculated, can it make additional discussion or provide interesting insight by comparing the average SMRmin with the water vapor mixing ratio observed by CFH? Also the case 2 is.

Reply: The authors calculated an ensemble trajectories for nine points around the observation site for cases 1 and 2. The minimum SMR for each trajectory is selected before air parcel met the cloud as Fig. 1 shows. For the 2009 case, the one sigma standard deviation of reconstructed water vapour of the ensemble of backward trajectories in the region of interest (378–384 K) agree well with observations. ERA5 reconstructed water vapour is below observed water vapour, but still in the one sigma standard deviation range. For the 2015 case, for both ERA-Interim and ERA5 the range of reconstructed water vapour is below the observations in the region of interest (376–382 K). However, in the region of interest the variability of reconstructed water vapour of ERA5 ensemble trajectories is much higher than ERA-Interim trajectories. This demonstrates the stronger dispersion of temperature values along ERA5 backward trajectories caused by the high resolution of ERA5 data. In contrast, ERA-Interim trajectories are going through nearly the same cold point temperature yield a much lower variability of reconstructed water vapour.

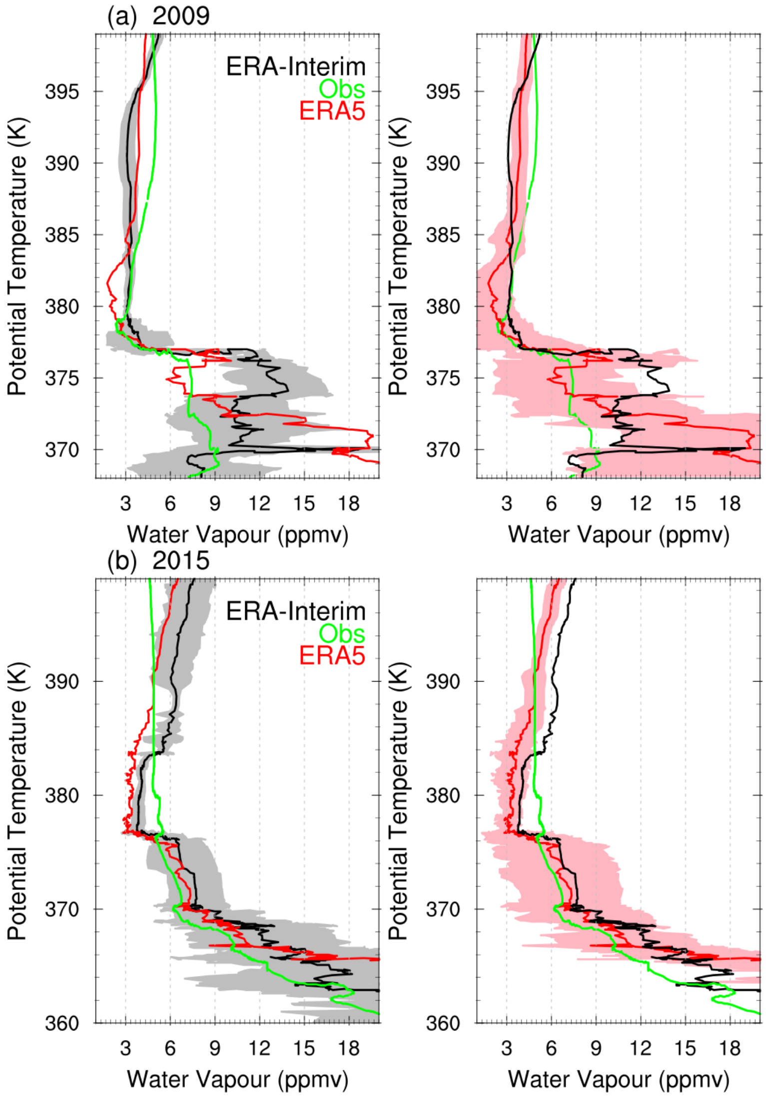

Figure 1. Water vapour profiles (green line) measured by CFH on (a) 8 August 2009 and (b) 10 August 2015 and mean reconstructed water vapour based on diabatic trajectories using ERA-Interim (black line) and ERA5 (red line) for 2009 and 2015. The grey/pink regions show the one sigma standard deviation range of the ensemble of backward trajectories.

References

Minnis, P., Smith, J. W. L., Garber, D. P., Ayers, J., and Doelling, D. R.: Cloud properties derived from GOES-7 for spring 1994 ARM intensive observing period using version 1.0.0 of ARM satellite data analysis program, NASA Ref. Publ., 1366, 1–58, 1995.

Wang, Z., Wang, Z., Cao, X., and Tao, F.: Comparison of cloud top heights derived from FY-2 meteorological satellites with heights derived from ground-based millimeter wavelength cloud radar, Atmos. Res., 199, 113–127, https://doi.org/10.1016/j.atmosres.2017.09.009, 2018.

Authors Reply to Anonymous Referee #3

The manuscript addresses the problem of the lifting of air by a tropical cyclone in the West Pacific during the Asian Monsoon and the resulting dehydration and low ozone layer in the lower stratosphere. The study consists in two case studies. It uses data from ozone and water vapor balloon profiles and MS data. Another interest is in the comparison of the new ERA5 and the ERA-Interim regarding Lagrangian trajectories near to a cyclone.
This work is interesting but somewhat misses to provide necessary details and I find the authors could have gone deeper into the analysis.

Reply: The authors appreciate the anonymous referee #3 for these useful comments. Please see below our responses point by point (*referees' comments in blue with italics font* and our response in black). Further, the revised manuscript is added highlighting in colour any changes compared to the ACPD version.

In 2.3 Provide information about the vertical sampling of the vertical interval and mention that the total diabatic heating rates, including latent heating are used (as it seems the case from the results).
Reply: We added "(total diabatic heating rates including clear-sky radiative heating, cloud radiative effects, latent heat release, as well as turbulent and diffusive heat transport; Fueglistaler et al., 2009) for the upper troposphere and stratosphere", "The vertical resolution in the UTLS is $\sim$ 1–1.5 km" and "with $\sim$400–500 m vertical resolution in the UTLS region" in section 2.3. For more information, please see the Fig.1 in this reply from Hoffmann et al. (2019).

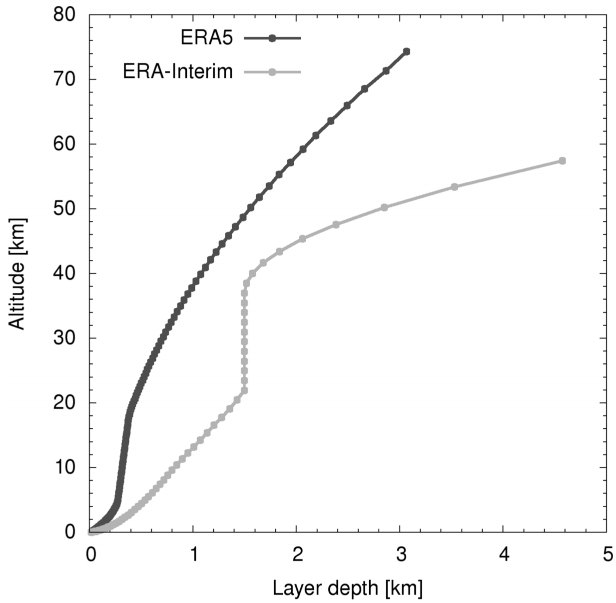

Figure 1. Vertical coverage and sampling of the ERA-Interim (light gray) and ERA5 (dark gray) reanalyses. Shown are layer depths and mid-layer altitudes calculated by means of the barometric formula using a constant scale height of 7 km and a surface pressure of 1013.25 hPa by courtesy of Hoffmann et al. (2019)

First case.

There is a layer of low ozone and low water vapor on 8 August near 365 K which could be a remain of that of the 4 August but no attention has been paid to it. The paper would be strengthened by showing the origin of that layer.

Reply: Thanks for this useful comment. The Fig. 2 in this reply shows the backward trajectory for air parcels at 364–367 K. It shows that air parcels with low ozone and low water vapour at 364–367 K from the western Pacific experienced a long-range transport along the ASM anticyclone after passing through the low temperature region over the South China Sea. Air parcels at 365 K get influence from the convective clouds associated with another tropical storm Goni. As Fig. 3 in this reply shows, air parcels dehydrated on 1 August 2009 when passing through the low temperature region. We added these two Figures in the appendix of the revised manuscript.

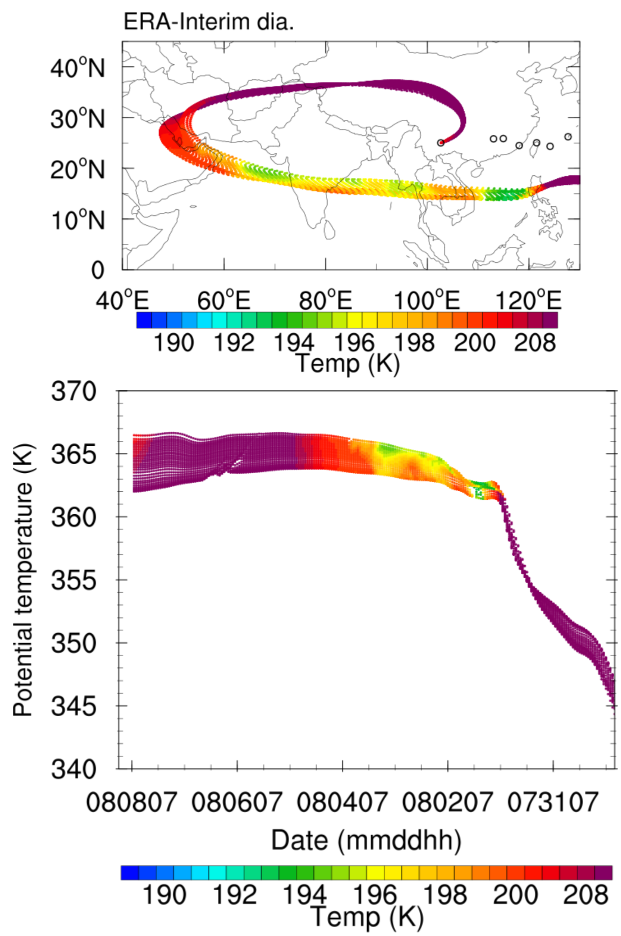

Figure 2. ERA-Interim diabatic trajectories for air parcels started along the measured balloon profile between 364 K and 367 K colour-coded by temperature in (top) longitude–latitude cross section and (bottom) as a function of time vs. potential temperature.

Lines 197-198: It seems that ERA5 predicts that the trajectories where inside the clouds but this fact is not exploited and the parcels are treated as unsaturated in the sequel.

Reply: We removed air parcels trajectories in clouds. Figs. 8 and 15 are updated.

What means, on line 203 that MLS water vapor is retrieved near the parcels location? The MLS value is the same for both ERA5 and ERA-Interim while the parcels are not located at the same level and can MLS see through the cloud anvils under which are located the ERA5 parcels? Therefore, how this value can be used as a reference to evaluate the dehydration? This is a crucial point in the analysis that deserves better description and justification.

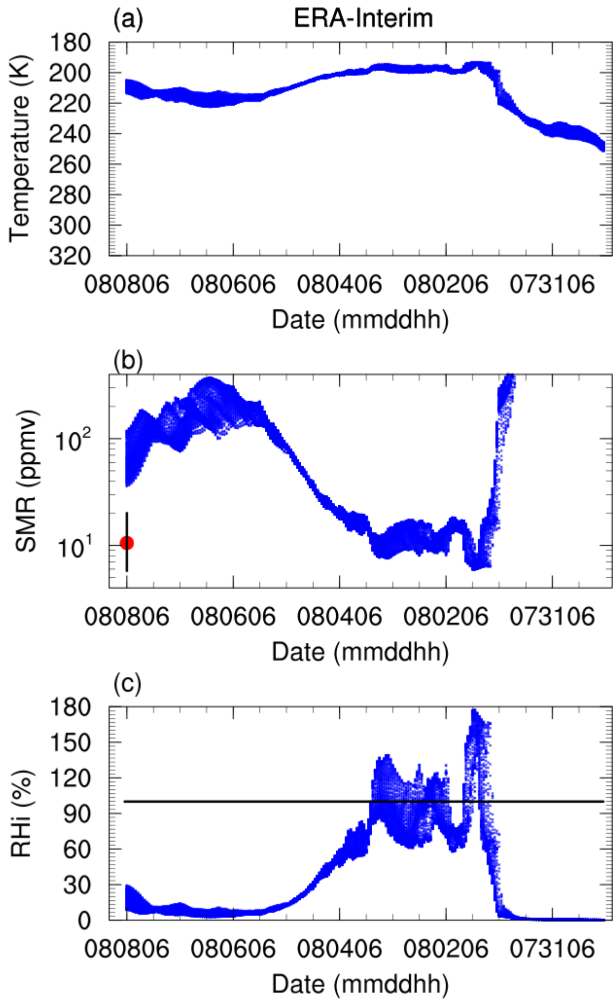

Figure 3. The time evolution of the temperature (blue dots), the saturation water vapour mixing ratio (SMR), relative humidity over ice ($\mathrm{RH_i}$) along 10-day backward trajectories of air parcels on 364–367 K from ERA-Interim diabatic trajectories.

Reply: The MLS track (triangles) is shown in Fig. 7a in the revised manuscript near the air parcels location at that time. After this time, air parcels become dry, before air parcels arrived at Kunming. According to the SMR and RHi in Fig. 8, air parcels experienced with clear sky before arriving at Kunming during 5–8 August. The CFH capture the dry air parcels. We check the water vapour value in addition from MIPAS, but unfortunately, the MIPAS track are far away from air parcels track on 4 August. Through MLS measurements are not the best reference, however, the best satellite data set available.

Line 209: It is unclear which water vapor is used for this estimate of the relative humidity. Is it the from the balloon flight of 8 August?

Reply: It is from the CFH instrument on board the balloon payload, we added this information in the revised manuscript.

On line 212, the authors mention that parcels get dry after passing through the lowest temperature region, but not attempt is made to see whether this can explain quantitatively the observed dehydration, even using a simple freeze-drying process relaxing to saturation. The analysis is too qualitative on this point (provided the previous question is also correctly answered).

Reply: The authors reorganized this paragraph "The relative humidity over ice ($\mathrm{RH_i}$) is calculated by dividing the water vapour mixing ratio from the CFH on by the SMR (Figs. 8e and f). If we assume that air parcels retain water vapor mixing ratio when it had been observed by the CFH, air parcels have experienced supersaturation ($\mathrm{RH_i}$ up to $180\,\%$) over the lowest temperature region according to ERA5 diabatic trajectories. ERA-Interim diabatic trajectories missed supersaturation, mainly due to higher temperatures along the trajectories of air parcels. CALIPSO total attenuated backscatter shows cirrus at the altitude of 17 km on 5 August around 18:00 UTC (not shown). The thin cirrus, in turn, provides evidence that dehydration is occurring over the lowest temperature region. As a conclusion, freezing and drying processes during the Lagrangian air parcel history contribute to the low water vapour mixing ratios found over Kunming in August 2009."

I find a bit confusing that the dates are oriented in opposite directions in figs. 4 and 8 on one side and 12 and 15 on the other side.
Reply: The authors reversed the X-axis in Figs. 8 and 15, to be consistent with Figs. 5 and 12.

Second case.

Here the MLS water vapor reference is retrieved at a date posterior to the exit of ERA5 trajectories from the clouds but details are still missing and again no attempt are made to quantitatively explain the dehydration.
Reply: We updated the Fig.15, only show the air parcels around the MLS track instead of all air parcels. The authors tried to find useful satellite data for this time and position including MIPAS and OMPAS. However, the authors could not find any water vapour data from satellite more suitable than MLS.

Looking at trajectories in fig.12, I do not find a convincing rise of 15 K of the low ozone layer between 5 and 10 August as required by fig. 11(b,c).
Reply: Thanks for this useful comment. The increase of 10 K can be seen in ERA-Interim diabatic and ERA5 kinematic/diabatic trajectories. The air parcels at 350–370 K on 5 August 2015 in Naha moved westward, however, not all of these air parcels arrived at Kunming. The backward trajectories only focus on the low ozone value at 370–380 K in Kunming in our manuscript.

Why trajectories are stopped at 330 K instead of 350 K as in the first case is not explained.
Reply: The bottom panels in Figs. 5 and 12 showing 7-day backward trajectory starting on different potential temperature levels. The range for the y-axis is chosen to highlight the temperature change along the trajectories. If the backward trajectories were stopped at 330 K for the case on 8 August 2009, it is hard to display the lower temperature region at 372 K. As a result, we show back trajectories between 350–400 K for the case on 8 August 2009 and 330–400 K for the case on 10 August 2015.

References

Fueglistaler, S., Legras, B., Beljaars, A., Morcrette, J.-J., Simmons, A., Tompkins, A. M., and Uppapla, S.: The diabatic heat budget of the upper troposphere and lower/mid stratosphere in ECMWF reanalyses, Q. J. R. Meteorol. Soc., 135, 638, https://doi.org/10.1002/qj.361, 2009.

Hoffmann, L., Günther, G., Li, D., Stein, O., Wu, X., Griessbach, S., Heng, Y., Konopka, P., Müller, R., Vogel, B., and Wright, J. S.: From ERA-Interim to ERA5: the considerable impact of ECMWF's next-generation reanalysis on Lagrangian transport simulations, Atmos. Chem. Phys., 19, 3097–3124, https://doi.org/10.5194/acp-19-3097-2019, 2019.

Dehydration and low ozone in the tropopause layer over the Asian monsoon caused by tropical cyclones: Lagrangian transport calculations using ERA-Interim and ERA5 reanalysis data

Dan Li[1,2], Bärbel Vogel[1], Rolf Müller[1], Jianchun Bian[2,3], Gebhard Günther[1], Felix Ploeger[1], Qian Li[2], Jinqiang Zhang[2,3], Zhixuan Bai[2], Holger Vömel[4], and Martin Riese[1]

[1]Institute of Energy and Climate Research: Stratosphere (IEK-7), Forschungszentrum Jülich, Jülich, Germany
[2]Key Laboratory of Middle Atmosphere and Global Environment Observation (LAGEO), Institute of Atmospheric Physics, Chinese Academy of Sciences, Beijing, China
[3]College of Earth Science, University of Chinese Academy of Sciences, Beijing, China
[4]Earth Observing Laboratory, National Center for Atmospheric Research, Boulder, CO, USA

Correspondence: Dan Li (lidan@mail.iap.ac.cn) and Jianchun Bian (bjc@mail.iap.ac.cn)

Abstract. Low ozone and ~~low~~ high water vapour mixing ratios are common features in the Asian summer monsoon (ASM) anticyclone, however, low ozone and low water vapour values were observed near the tropopause over Kunming, China ~~were observed~~ within the ASM using balloon-borne measurements performed during the SWOP (sounding water vapour, ozone, and particle) campaign in August 2009 and 2015. Here, we investigate low ozone and water vapour signatures in the upper troposphere and lower stratosphere (UTLS) using FengYun-2D, FengYun-2G, Aura Microwave Limb Sounder (MLS) satellite measurements and backward trajectory calculations~~driven by both ERA-Interim and ERA5 reanalysis data~~. Trajectories with kinematic and diabatic vertical velocities were calculated using the Chemical Lagrangian Model of the Stratosphere (CLaMS) trajectory module driven by both ERA-Interim and ERA5 reanalysis data.

All trajectory calculations show that air parcels with low ozone and low water vapour values in the UTLS over Kunming measured by balloon-borne instruments originate from the western Pacific boundary layer. Deep convection associated with tropical cyclones over the western Pacific transports ~~boundary air parcels with low ozone into the~~ ozone-poor air from the marine boundary layer to the cold tropopause region. Subsequently, these air parcels are mixed into the strong easterlies on the southern side of the Asian summer monsoon anticyclone. Air parcels are dehydrated when passing the lowest temperature region (<190 K) ~~over the western Pacific during quasi-horizontal advection~~at the convective outflow of tropical cyclones. However, trajectory calculations show different vertical transport via deep convection depending on the employed reanalysis data (ERA-Interim, ERA5) and vertical velocities (diabatic, kinematic). Both the kinematic and the diabatic trajectory calculations using ERA5 data show much faster and stronger vertical transport than ERA-Interim primarily ~~due to~~ because of ERA5's better spatial and temporal resolution, ~~likely resolving more convective events .~~ which likely resolves convective events more accurately. Our findings show that the interplay between the ASM anticyclone and tropical cyclones has a significant impact on the chemical composition of the UTLS during summer.

1 Introduction

The Asian summer monsoon (ASM) anticyclone plays an important role in transporting air masses from the troposphere into the stratosphere (e.g. Chen et al., 2012; Garny and Randel, 2016; Randel et al., 2010; Vogel et al., 2019). Air masses within the ASM anticyclone are impacted by surface sources from the western Pacific, India, Southeast Asia and the Tibetan Plateau (Bergman et al., 2013; Park et al., 2008; Tissier and Legras, 2016; Vogel et al., 2015). Recently, Höpfner et al. (2019) have reported observations that indicate upward transport from ground sources of ammonia (NH_3) to greater altitudes with subsequent formation of ammonium nitrate (NH_4NO_3) during further ascent in the ASM anticyclone. This is further confirmed by satellite observations of air pollution from biomass burning (e.g. carbon monoxide, hydrogen cyanide, ethane) which clearly support the idea of convective uplift from the surface to the tropopause layer within the ASM anticyclone ~~(Park et al., 2008; Yan and Bian, 2015)~~(Park et al., 2008; Chen et al., 2012; Bergman et al., 2013; Yan and Bian, 2015). Using trajectory calculations, Chen et al. (2012) demonstrate that 38% of the air masses at tropopause height within the ASM region are from the western Pacific region and South China Sea. Bergman et al. (2013) also show that 36.1% of air parcels at 100 hPa in the monsoon region originate from the western Pacific based on diabatic trajectory calculations.

Convection in ~~the~~ tropical cyclones (e.g. typhoons in the western Pacific) can lift air masses from the marine boundary layer into the tropopause layer (Li et al., 2017; Minschwaner et al., 2015; Pan et al., 2016; Vogel et al., 2014). Tropospheric ozone can be decomposed by halogen induced photochemical reactions in the tropical marine boundary layer (von Glasow et al., 2002). As a result, low ozone values are distributed over at least several thousand kilometers over the tropical oceans (Read et al., 2008a) . Low ozone values are sometimes measured in the upper troposphere within typhoons or hurricanes (Cairo et al., 2008; Fu et al., 2013), due to fast vertical transport caused by tropical cyclones. Minschwaner et al. (2015) find that hurricane Henriette uplifted air with low ozone from the boundary layer in the central and eastern Pacific to the upper troposphere with subsequent transport to Socorro (North America) according to balloon-borne ozonesonde and satellite measurements. Newton et al. (2018), using aircraft measurements in Guam, show that low ozone values (20 ppbv) in the tropical tropopause layer (TTL) are caused by deep convection, which has lifted ozone-poor boundary-layer air to the TTL over the western Pacific in 2014.

The lowest temperatures in the TTL are often found over the western Pacific. When air parcels are transported horizontally via the lowest temperature tropopause region (cold trap) over the western Pacific in winter, dehydration occurs (Holton and Gettelman, 2001). Read et al. (2008b), using model calculations and ~~the~~ Aura Microwave Limb Sounder (MLS) measurements, show that water vapour is controlled by the lowest temperature in the TTL, ~~that is called,~~ i.e. by in-situ freeze-drying.

In-situ observations from the Soundings of Ozone and Water in the Equatorial Region (SOWER) campaign in winter show a clear correspondence between dry air parcels and low temperatures during advection in the TTL over the western Pacific (Hasebe et al., 2007). The match technique was applied to quantify the features of dehydration or hydration for air parcels in the TTL (Hasebe et al., 2013; Inai et al., 2013). The relative humidity with respect to ice (RH_i) of 146±19%, a threshold of ice nucleation, indicates the development of ice clouds. Dehydration is ongoing until RH_i decreases to 75±23% between 350 K to 360 K (Inai et al., 2013). Cold-trap dehydration is accompanied by slow ascent in the TTL and quasi-horizontal advection between 360 K and 380 K (Hasebe et al., 2013). Lagrangian trajectory simulations also show that water vapour mixing ratios transported into the stratosphere from the South China and Philippine Seas are lower ~~compared to~~ than those transported from the South Asian subcontinent and the Southern Slope of the Himalayas and the Tibetan Plateau (Wright et al., 2011). Deep convection contributes to low temperature regions in the subtropical lower stratosphere, and leads to a dry stratosphere (Randel et al., 2015).

Low water vapour mixing ratios below 2 ppmv were observed at the cold point tropopause (370–380 K) during the Stratospheric-Climate Links with Emphasis on the Upper Troposphere and Lower Stratosphere (SCOUT-O3) air craft campaign in November and December 2005 over Darwin, Australia (Schiller et al., 2009). These low water vapour mixing ratios are primarily determined by effective freezing-drying near the tropopause caused by deep convection associated with the cumulonimbus system Hector.

Li et al. (2017) found that tropical cyclones that occurred over the western Pacific uplifted marine boundary layer air masses with low ozone to the ASM anticyclone, using balloon measurements and trajectory calculations. In general, typhoons decrease ozone values near the tropopause over the western Pacific. However, hitherto the variability of water vapour concentrations in the upper troposphere and lower stratosphere (UTLS) region has not been analysed in detail. Using balloon-borne measurements, MLS data, and the Chemical Lagrangian Model of the Stratosphere (CLaMS) trajectory calculations, we will investigate how ~~the~~ tropical cyclones impact water vapour structures in the UTLS region over Kunming. This paper is organized as follows: Sect. 2 describes the balloon measurement data and the trajectory calculations with the CLaMS model. In Sect.3, we will present two-case studies where dehydration is found in the measurements. A comparison of diabatic and kinematic trajectory calculations driven by both ERA-Interim and ERA5 reanalysis data will be presented as well. A summary will be given in the final section.

2 Measurements and trajectory calculations

2.1 Balloon-borne measurements

Vertical profiles of temperature, ozone, and water vapour were measured over Kunming (25.01° N, 102.65° E, above sea level (asl.) 1889 m), China, in August 2009 and 2015 during the SWOP (sounding water vapour, ozone, and particle) campaign (e.g. Bian et al., 2012; Li et al., 2017, 2018). In 2009, 11 balloons were launched during the period 7–13 August; seven and four balloons were launched in the daytime and at night (around 10:00 and 22:30 local time, UTC+8). Detailed information about the launches is provided by Bian et al. (2012, see table S1). In 2015, 12 balloons were launched around 22:30 (local time, UTC+8) from 3 to 18 August. Profiles of temperature, pressure, relative humidity, and winds were measured by Vaisala RS80 radiosondes in 2009 and iMet radiosondes in 2015. Profiles of ozone and water vapour mixing ratios were measured by an electrochemical concentration cell (ECC) ozonesonde (Komhyr et al., 1995) and a cryogenic frost point hygrometer (CFH) (Vömel et al., 2007), respectively. Data are transmitted to Kunming ground receiving station ∼100 minutes and are recorded each second. The ozone and water vapour precision in the troposphere is 10% and 5%, respectively (Vömel et al., 2016).

The (saturation) water vapour mixing ratio is calculated from the (ambient) frost point temperature using the Hyland–Wexler equation (Hyland and Wexler, 1983) for liquid water and from the Goff–Gratch equation (Goff and Gratch, 1946; Murphy and

Koop, 2005) for ice water. The match technique, means that the same air parcel is observed more than once (Hasebe et al., 2013; Inai et al., 2013). Then the difference of water vapour values between these observation times was applied to quantify the features of dehydration or hydration for air parcels during horizontal advection in the TTL.

Ozone profiles for Naha (26.21° N, 127.69° E, asl. 28.1 m), Okinawa Island, Japan during the period of 2008–2017 were obtained from the World Ozone and Ultraviolet Radiation Data Centre (Naja and Akimoto, 2004). Naha station is located approximately 2500 km east of Kunming, and these two sites are nearly on the same zonal line. Profiles on 4 August 2009, 05:30 UTC and on 5 August 2015 from Naha will be presented in sections 3.1.2 and 3.2.2, respectively.

The upper air soundings of Chenzhou, Ganzhou, Xiamen, Taipei, and Ishigakijima in August 2009 and Haikou, Wuzhou, Hongkong, Shantou, Laoag, and Ishigakijima in August 2015 were used in this paper. The data are downloaded from the University of Wyoming. Balloons were launched routinely, every twice per day at 00:00 UTC and 12:00 UTC. They provide profiles of temperature, pressure, relative humidity, and wind vector from the surface to 30 km.

2.2 Satellite data

Microwave Limb Sounder (MLS) measurements are used to validate ozone and water vapour profiles in the tropopause layer over the western Pacific. MLS level 2 version 4.2x standard atmospheric product data are used for 4 August 2009 and the period of 31 July–10 August 2015. MLS provides ozone with 10 pressure levels ranging from 261 hPa to 46 hPa (9.5–21.5 km) along the orbit track (Livesey et al., 2018). Precision on individual ozone profiles is within 5% or better in the lower stratosphere, and is approximately 15%–25% at 100 hPa, while with poor behavior at low latitudes in the upper troposphere. The mean deviation is lower than 20% between the MLS and the ECC ozone values in the upper troposphere over the Tibetan Plateau (Shi et al., 2017).

The FengYun-2D ("Feng and Yun" means "winds and clouds" in Chinese), or FY-2D in acronym and FY-2G are the geostationary meteorological satellite series of China, organized and operated by the national satellite meteorological center of CMA (China Meteorological Administration). FY-2D was launched on 8 December 2006, and carried a payload with a five-channel Stretched Visible and Infrared Spin Scan Radiometer (S-VISSR) to track cloud motion. Long wave infrared (10.3–11.3 μm) with a spatial resolution of 5 km is used to detect cloud moving. Here, we used the FY-2D blackbody brightness temperature ~~(TBB)~~ product to determine the cloud top temperature. FY-2G was launched on 31 December 2014 and carried a S-VISSR. ~~We use cloud top temperature (CTT) to detect the cloud motion and location~~The brightness temperature was also used.

2.3 Trajectory calculations based on ERA-Interim and ERA5 reanalysis data

Diabatic and kinematic backward trajectories along two balloon's ascending paths over Kunming on 8 August 2009 and 10 August 2015 were calculated using the CLaMS trajectory module ~~(Konopka et al., 2004; McKenna et al., 2002; Pommrich et al., 2014)~~ (McKenna et al., 2002; Konopka et al., 2004; Pommrich et al., 2014). The CLaMS kinematic trajectory calculations employ pressure (p) as the vertical coordinate and omega (ω) as vertical velocity. In contrast, the diabatic trajectory calculations employ a hybrid σ-potential temperature coordinate (Pommrich et al., 2014) and the diabatic vertical velocity derived from total heating rates. Note, that above $\sigma = p/p_s$=0.3, hence throughout the stratosphere and upper troposphere, the vertical coordinate is just potential temperature. Diabatic calculations have important advantages (total diabatic heating rates including clear-sky radiative heating, cloud radiative effects, latent heat release, as well as turbulent and diffusive heat transport; Fueglistaler et al. 2009) for the upper troposphere and stratosphere (e.g. Ploeger et al., 2010, 2011; Schoeberl et al., 2003; Schoeberl and Dessler, 2011). The dynamic fields from the European Centre for Medium-range Weather Forecasts (ECMWF) interim reanalysis (ERA-Interim) (Dee et al., 2011) and ECMWF's next-generation reanalysis ERA5 (Hersbach and Dee, 2016) are used to drive the CLaMS ~~model~~trajectories. ERA-Interim input data ~~is~~ are recorded on a $1^\circ \times 1^\circ$ grid every 6 hours, on 60 hybrid levels from about 1013.25 hPa to 0.1 hPa. The vertical resolution in the UTLS is $\sim$1–1.5 km. The ERA5 input data is provided on a $0.3^\circ \times 0.3^\circ$ grid every hour on 137 hybrid levels from the surface to 0.01 hPa, with $\sim$400–500 m vertical resolution in the UTLS region. The ERA5 ~~has~~ date have a much higher spatial and temporal resolution than ERA-Interim, especially in the upper troposphere and lower stratosphere ~~(Hoffmann et al., 2019, see Fig. 1)~~(Hoffmann et al., 2019, as shown in Fig. 1). The horizontal wind fields show similar structure at 150 hPa between ERA-Interim and ERA5 reanalysis data (Fig. A1). The vertical velocities from ERA5 show finer spiral structures ~~compared to that from~~ than ERA-Interim vertical velocities at 150 hPa in regions of tropical cyclones (Fig. 1). Stronger negative ω in ERA5 corresponds to ascending motion around the convection centers associated with tropical cyclones as shown in the right column of Fig. 1. The outflow of deep convection is clearly much stronger on 6 August 2009 than on other days based on ERA5 reanalysis data.

3 Results

3.1 Case 1: 8 August 2009

All vertical profiles of temperature, ozone, and water vapour mixing ratios over Kunming in August 2009 are shown in Fig. 2. The minimum temperature of 192.3 K occurs on 8 August (Fig. 2a). The ~~lapse rate tropopause~~ World Meteorological Organization (WMO) tropopause (WMO, 1957) potential temperature on 8 August is located at 381.3 K. Ozone mixing ratios in the upper troposphere ranged from 40 ppbv to 120 ppbv in August 2009. Ozone mixing ratios observed on 8 August show low values in the potential temperature layer between 376 K and 384 K, with a minimum value of 35 ppbv around 378 K (Fig. 2b). Simultaneously, water vapour near the tropopause on 8 August is also very low, around 2.5 ppmv at 378 K (Fig. 2c). Low ozone and low water vapour mixing ratios near the tropopause on 8 August are strongly correlated, marked by the shaded regions in Fig. 2. ~~It is necessary to mention~~ The ozone and water vapour around 378 K are lower by 70% and 40% in contrast to monthly mean value, respectively (Fig. A2). Low ozone (60 ppbv) and low water vapour (6 ppmv) values are also observed at another layer near 365 K on 8 August 2009. The relative difference for ozone and water vapour is about −40% (Fig. A2). The detailed information for this low ozone and water vapour layer will be shown in Appendix A. Note that Bian et al. (2012) highlight ~~this~~ these low ozone and low water vapour values using the same observation data. They argue that the rapid convective uplift and the low temperature near the tropopause are the reason for these coinciding low ozone and low water vapour values. However, they only offer limited explanation on the detailed reasons, which are investigated and discussed in the following subsections.

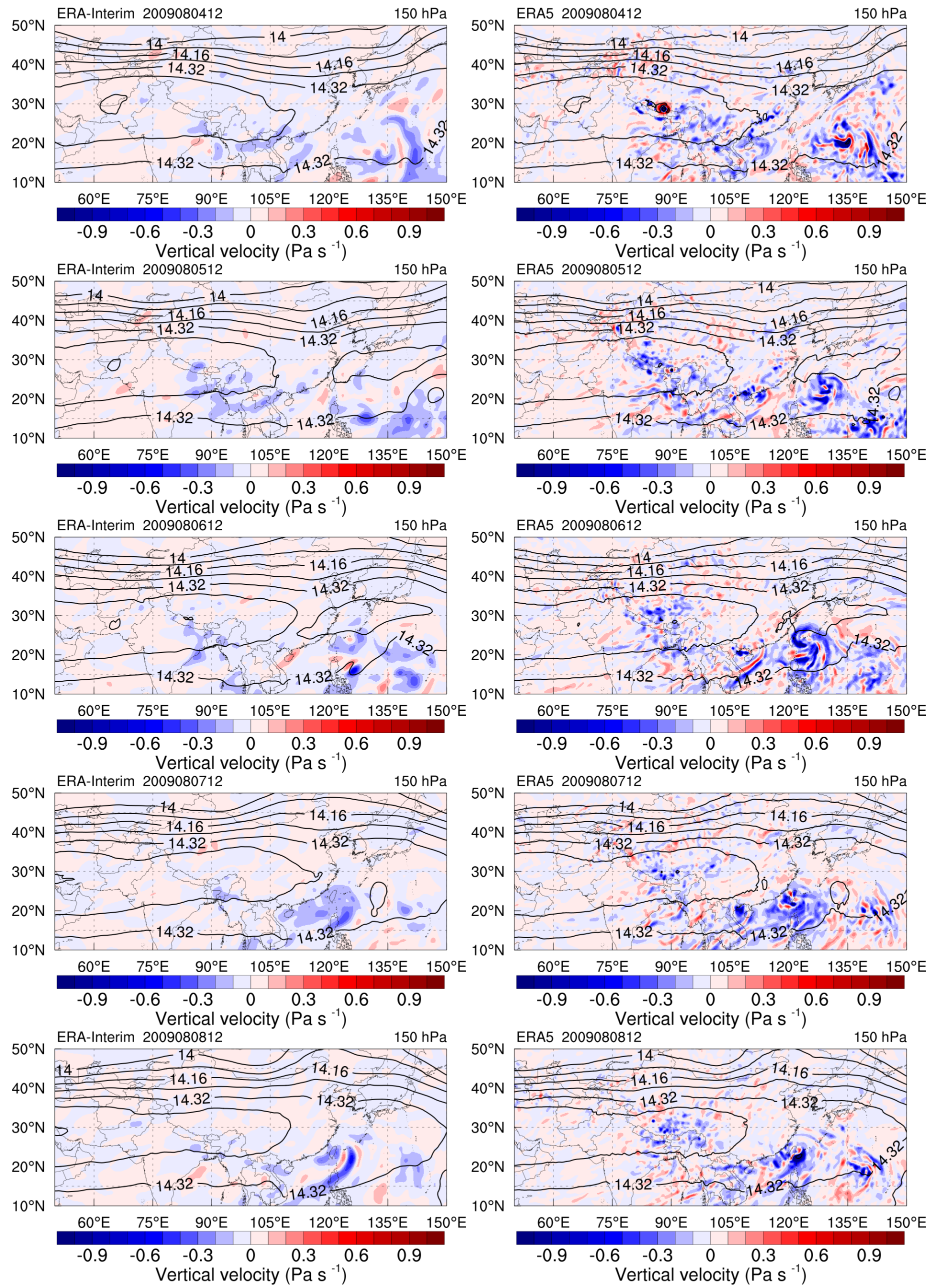

Figure 1. Geopotential height (black lines, gpkm) and vertical ω velocities (shaded, $\mathrm{Pa\,s^{-1}}$) at 150 hPa on 4, 5, ~~and~~ 6, 7, and 8 August 2009 from ERA-Interim (left) and ERA5 (right).

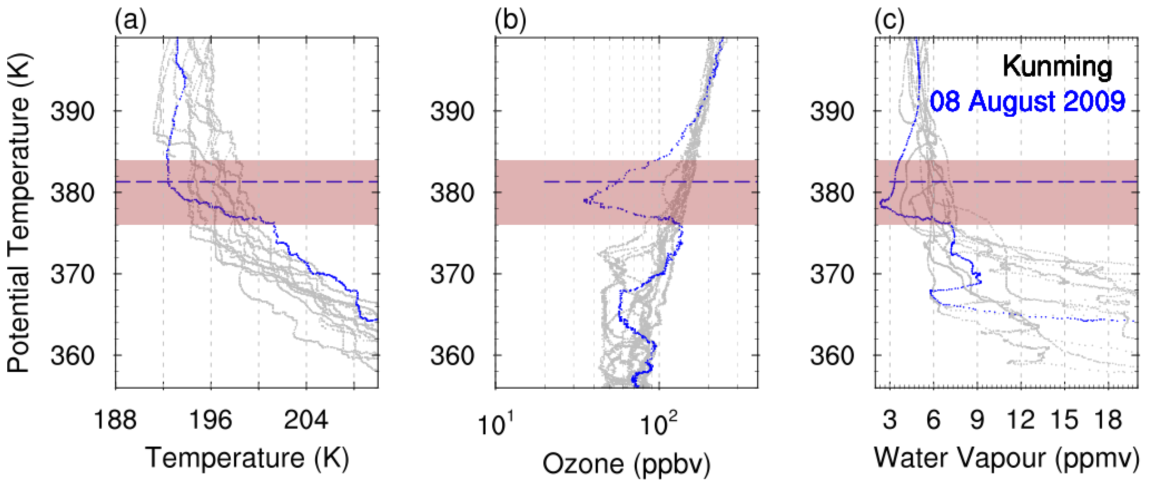

Figure 2. All vertical profiles of (a) temperature, (b) ozone mixing ratios (OMRs), and (c) water vapour over Kunming in August 2009. The profile on 8 August is marked as blue line. The horizontal blue dashed line marks the lapse rate tropopause on 8 August. The shading region denotes the low ozone and low water vapour mixing ratios region.

3.1.1 Background meteorology

Figure 3 shows the 5-day average (4–8 August 2009) of the geopotential height isolines (>16.7 gpkm) at the 100 hPa pressure level with the temperature (shaded), horizontal wind vector, and tracks of typhoon Morakot from the ERA-Interim reanalysis data. Isolines are used to denote the scope of the ASM anticyclone. Morakot formed early on 2 August, within a monsoon trough about 1000 km east of the Philippines. Morakot moved westward since 4 August, and arrived at the south of Naha on 6 August. During the period 4–8 August 2009, the southeastern edge of the ASM anticyclone was located above the top of the typhoon and covered the lowest temperature region (<192 K). Similar results can also be obtained from the ERA5 analysis data (not shown).

3.1.2 Low ozone in the tropopause layer

A balloon was launched in Naha, Japan on 4 August 2009 before the typhoon Morakot passed through this site. Low ozone values (35 ppbv) appeared at the layer between 360 K and 370 K (Fig. 4a). The observed mean ozone value of 10 years (2008–2017) in this layer is about 80–120 ppbv. The balloon on 8 August in Kunming also captured the extremely low ozone structure, but at the layer between ∼376–384 K. The altitude of the low ozone appearing in Kunming on 8 August is higher than that in Naha on 4 August 2009. Low ozone values near the tropopause within the ASM anticyclone were also found in Lhasa in 2013 (Li et al., 2017), which are caused by the combination of the rapid vertical transport from typhoon convection and the horizontal transport at the edge of the ASM anticyclone. The ERA-Interim and ERA5 temperature and ozone data were interpolated to the balloon tracks on 8 August. ~~Note that the balloon data were not assimilated into the ERA5 and ERA-Interim reanalysis.~~ Compared to balloon observation, the ERA5 temperature profile shows a lower value than ERA-Interim temperature

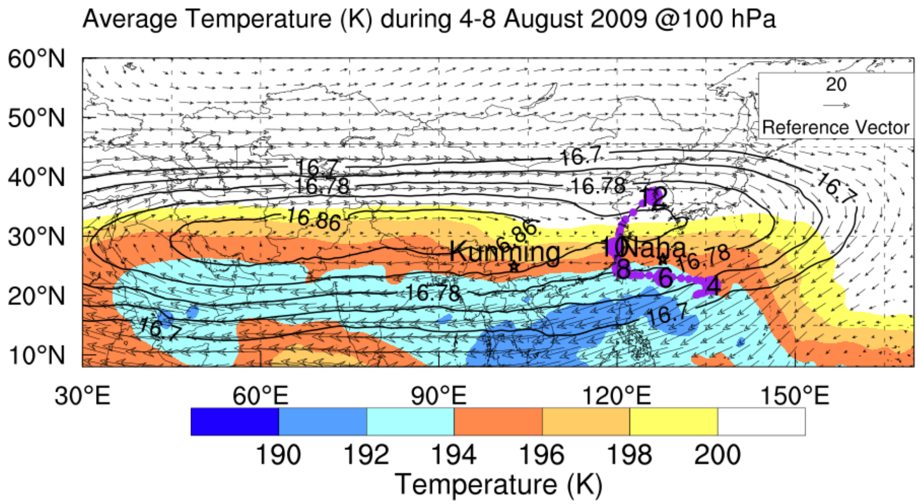

Figure 3. (a) The 5-day average (4–8 August) of geopotential height (black lines, >16.70 gpkm), temperature (shaded, K), and wind speed (vectors, $\mathrm{m\,s^{-1}}$) from ERA-Interim at the 100 hPa pressure with the tracks of typhoon Morakot (purple dots). The numbers in purple dots indicate days in August 2009. The black stars mark the locations of Naha and Kunming.

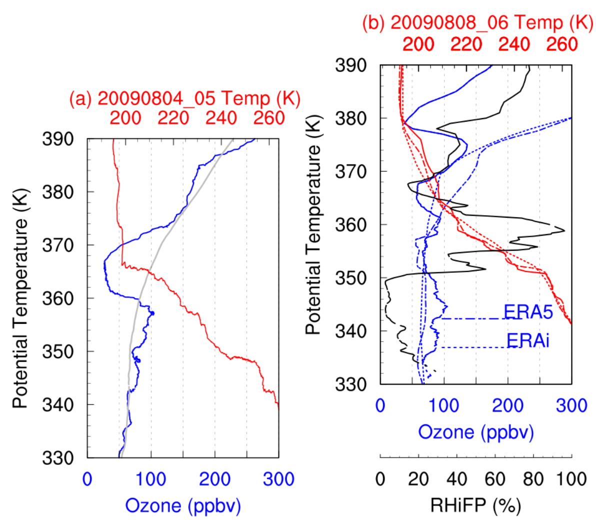

Figure 4. Profiles of ozone (blue), mean ozone (grey), relative humidity ~~(RH~~ from ~~radiosondes, and RHFP from~~ CFH (RH$_i$FP, black), and temperature (red) in (a) Naha on 4 August and (b) Kunming on 8 August (solid line–observation, dashed line–ERA-interim, dash-dotted line–ERA5).

on 8 August 2009. Both the ERA-Interim and ERA5 ozone profiles show large positive deviations in the tropopause layer with respect to observations.

3.1.3 Low temperatures and dehydration in the western Pacific

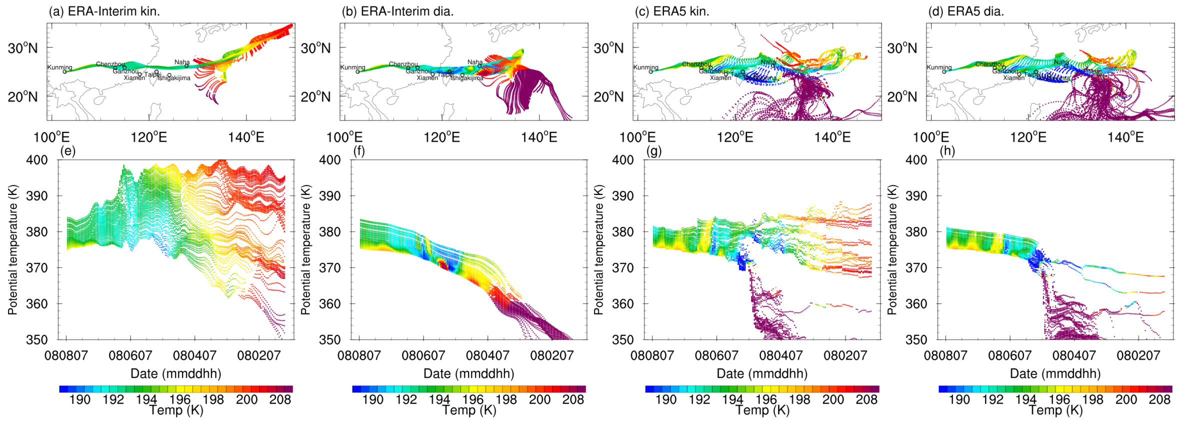

Figure 5. ERA-Interim kinematic (a, e) and diabatic (b, f), and ERA5 kinematic (c, g) and diabatic (d, h) 7-day backward trajectories for air parcels started along the measured balloon profile between 376 K and 384 K colour-coded by temperature in (top) longitude–latitude cross section and (bottom) as a function of time vs. potential temperature.

Figure 5 shows 7-day backward trajectories of air parcels with low ozone and low water vapour between 376 K and 384 K initialized on 8 August 2009 in Kunming. A comparison of diabatic and kinematic trajectory calculations is shown based on ERA-Interim and ERA5 reanalysis data. Air parcels originating from the western Pacific were transported to the tropopause layer under significant influence of typhoon convection, then affected by the easterly wind flow at the south flank of the ASM anticyclone. Subsequently, air parcels moved horizontally via Naha, Ishigakijima, Taipei, Xiamen, Ganzhou, Chenzhou, then to Kunming according to backward trajectories projected on the map (Figs. 5a–d). The convection associated with typhoon Morakot transported ozone-poor air from the marine boundary layer to the tropopause layer, these low ozone values were captured as these air parcels moved westward to Naha and Kunming. Trajectories from ERA-Interim and ERA5 reanalysis data show the lowest temperature region ($<$190 K) in the tropopause layer over Taiwan and Ishigakijima except the ERA-Interim kinematic trajectories. The main difference of the backward trajectories is the vertical transport over the western Pacific, where tropical cyclones may occur (Figs. 5e–h). Large-scale slow descent processes ($\sim$1–2 K/day) can only be seen clearly from ERA-Interim kinematic trajectories (Fig. 5e). This is consistent with Ploeger et al. (2011) who showed much stronger vertical dispersion for ERA-Interim kinematic trajectories. Although all of the backward trajectories display the vertical transport within deep convection, the timescale and the strength of air parcels' vertical transport processes are different according to the backward trajectories as a function of time and isentrope. The timescale of the vertical transport from the lower troposphere to the tropopause layer based on ERA-Interim diabatic trajectories is about 4 days from 1 August to 5 August (Fig. 5f). In contrast, the vertical transport timescale based on the ERA5 kinematic and diabatic trajectory calculations is 2 days around 4–5 August (Figs. 5g and h). Both the kinematic and diabatic trajectories from ERA5 display faster vertical transport than ERA-Interim. It is very likely that ERA5 resolves more convective events (e.g. Fig. 1), due to its better spatial and temporal resolution.

Hoffmann et al. (2019) have also shown that tropical cyclones are represented better in ERA5, compared to ERA-Interim reanalysis data.

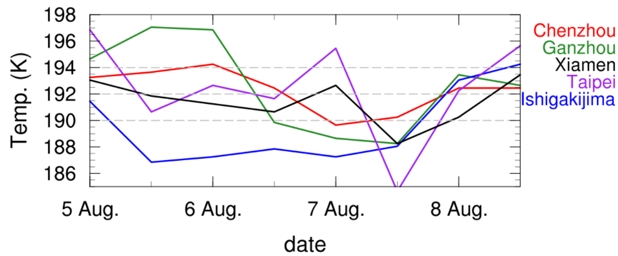

Figure 6. The time series of the lowest temperature in the tropopause layer for Chenzhou, Ganzhou, Xiamen, Taipei, and Ishigakijima.

The time series of the lowest temperature from Chenzhou, Ganzhou, Xiamen, Taipei, and Ishigakijima are shown in Fig. 6 based on upper air soundings. The balloon measurement at Taipei captured the lowest temperature (186 K) during the period 5–7 August 2009 near the tropopause. ERA-Interim kinematic trajectories missed the lowest temperature values compared to the upper air soundings, and do not show the strong updraft in tropical cyclones. Therefore, ERA-Interim kinematic trajectories will not be considered further in the following.

Figure 7 shows the blackbody brightness temperature from infrared radiation (IR) channel of FY-2D. The blue colour marks the low brightness temperature region, which means that deep convection with a high cloud top occurred in the centre of a tropical cyclone. Air parcels were located right above deep convection of typhoon Morakot on 4 August according to the ERA5 kinematic and diabatic trajectories (Fig. 7a). The ERA-Interim diabatic trajectories were located further at the northern edge of the typhoon. One day later, all trajectories arrived at the Naha site over the western Pacific region (Fig. 7b). Air parcels continue to move westward towards Kunming under clear sky conditions during the last two days (Figs. 7c and d).

In order to investigate the variation of water vapour mixing ratios at the top of the typhoon convection, Figs. 8a and b show the temperature along the 4-day backward trajectories of air parcels at 376–384 K on 8 August 2009 with the brightness temperature from FY-2D (grey dots). The y-axis of Figure 8 represents a vertical altitude coordinate (decreasing temperatures). The brightness temperature was interpolated from FY-2D onto the locations of air parcels from the ERA-Interim and ERA5 diabatic trajectory calculations and was used to ~~denote~~ describe the cloud top temperature. ERA-Interim diabatic trajectories show that air parcels were located right above the deep convection according to the brightness temperature from FY-2D from 5 August, 00:00 UTC to 6 August, 12:00 UTC (Fig. 8a). Compared to ERA-Interim trajectories, ERA5 diabatic trajectory calculations show different results, in particular that the brightness temperature from FY-2D is lower than air parcels' temperature (187 K) on 4 August (Fig. 8b). In other words, the cloud top is higher than the air parcels' altitude. As a result, these air parcels will not be used for analysing the water vapour variation. The saturation water vapour mixing ratio (SMR) is estimated using the temperature along the backward trajectories of air parcels according to the Goff–Gratch equation (Goff and Gratch, 1946; Murphy and Koop, 2005). The minimum SMR appears on 5 August, at 12:00 UTC, corresponding to the lowest temperature region (Figs. 8c and d). Before air parcels enter the lowest temperature region, several profiles of water vapour from the MLS

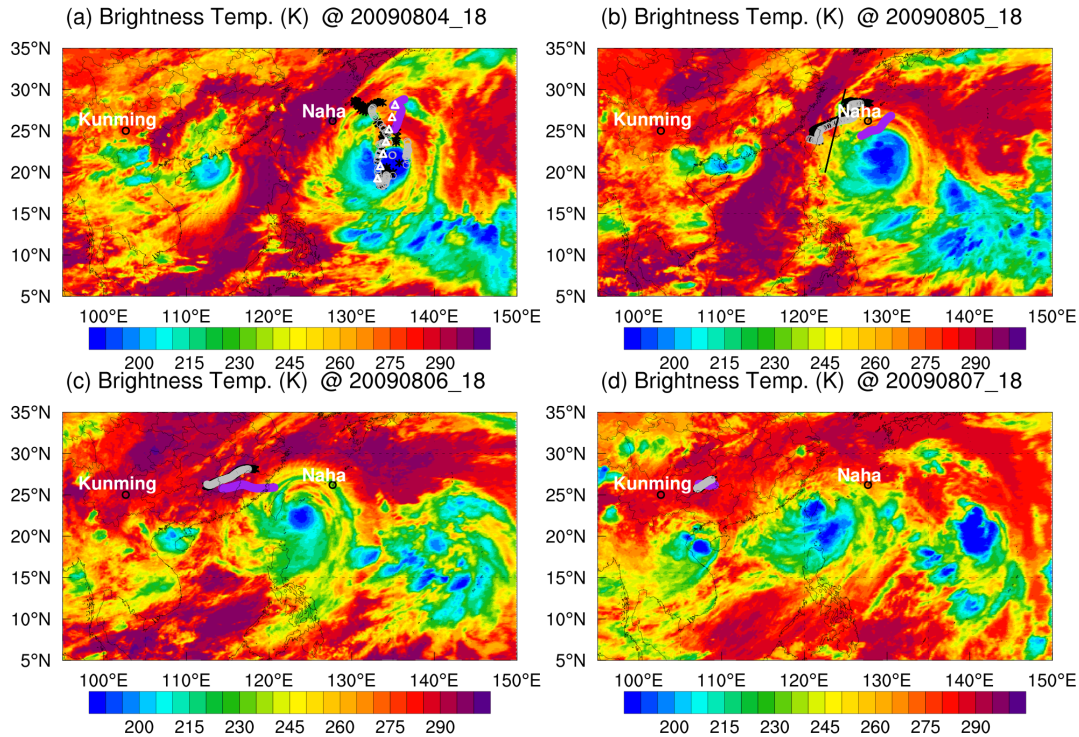

Figure 7. Brightness temperature (K) from IR channel of FY-2D on (a) 4 August, 18:00 UTC, (b) 5 August, 18:00 UTC, (c) 6 August, 18:00 UTC, and (d) 7 August 2015, 18:00 UTC with air parcels' locations based on backward trajectories (grey circles–ERA5 diabatic, black asterisk–ERA5 kinematic, purple circles–ERA-Interim diabatic). White triangles mark the MLS tracks (a) and the black line denotes the ground track of CALIPSO (b).

satellite near to the air parcels' locations (Figs. 7a) are used with the mean value of 5±0.3 ppmv marked with a red dot (left-hand side) of Figs. 8c and d on 4 August, 17:30 UTC at 100 hPa. Three days later, the mean water vapour mixing ratio of the same air parcels are about 3 ppmv, marked with red dot (right-hand side). The minimum ~~SMR~~ water vapor mixing ratio observed by CFH is approximate 2.7 ppmv in Kunming on 8 August, after air parcels pass through the lowest temperature region from 5 August 07:00 UTC to 6 August, 12:00 UTC in 2009. Although MLS water vapour profiles usually show mean values of a 3–4 km wide vertical layer, the value corroborates that air parcels become dry, with water vapour mixing ratios decreasing from 5 ppmv to 3 ppmv. The relative humidity over ice (RH_i) is calculated by dividing the water vapour mixing ratio from the CFH by the SMR (Figs. 8e and f). ~~Air parcels~~ If we assume that air parcels retain water vapor mixing ratio when it had been observed by the CFH instrument on board the balloon payload, air parcels have experienced supersaturation (RH_i up to 180 %) over the lowest temperature region according to ERA5 diabatic trajectories. ERA-Interim diabatic trajectories missed supersaturation, mainly due to higher temperatures along the trajectories of air parcels. ~~Air parcels become dry after they passed through the lowest temperature region.~~ CALIPSO total attenuated backscatter shows cirrus at the altitude of 17 km on 5 August around 18:00 UTC (not shown). The thin cirrus, in turn, provides evidence that dehydration is occurring over the

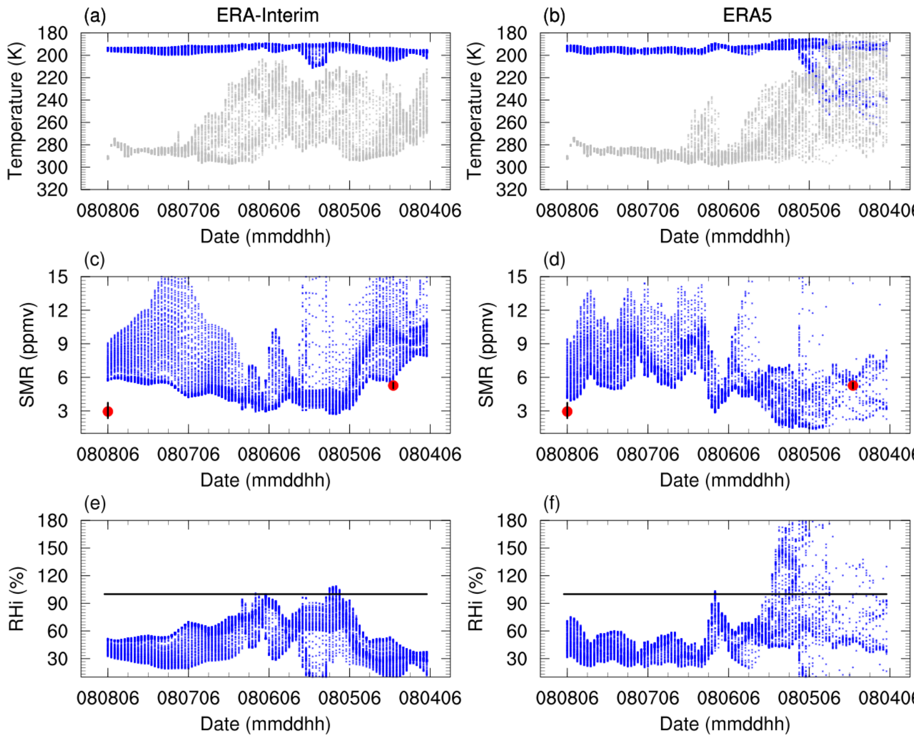

Figure 8. The time evolution of (a, b) the temperature (blue dots) and brightness temperature from FY-2D (grey dots), (c, d) the saturation water vapour mixing ratio (SMR), (e, f) relative humidity over ice (RH_i) along 4-day backward trajectories of air parcels on 376–384 K from (a, c, and e) ERA-Interim and (b, d, and f) ERA5 diabatic trajectories. The red dots in c and d denote the water vapour mixing ratio from MLS (left-hand side) and balloon observation (right-hand side).

lowest temperature region. As a conclusion, ~~freezing~~ ice formation and drying processes during the ~~lagrangian~~ Lagrangian air parcel history contribute to the low water vapour mixing ratios found over Kunming in August 2009.

3.2 Case 2: 10 August 2015

Vertical profiles of temperature, ozone, and water vapour measured over Kunming in August 2015 are shown in Fig. 9. The potential temperature of the lapse rate tropopause on 10 August 2015 is about 383.7 K. The tropopause height in Kunming is usually higher than in the other regions at the same latitude, ~~based on~~ because of its location within the ASM anticyclone (Bian et al., 2012). On 10 August, the temperature between 365 K and 376 K shows higher values than on other days. Ozone mixing ratios ~~near the tropopause~~ in August 2015 show a good agreement near the tropopause, except for 10 and 11 August, when much lower ozone mixing ratios are recorded. The ozone vertical profile observed on 10 August 2015 shows extremely low ozone mixing ratios between 364 K and 390 K, with a minimum value of 22 ppbv around 368 K. ~~These~~ Similarly low ozone values were ~~also~~ measured on 11 August 2015, with a minimum ozone value of 30 ppbv near 373 K. Low ozone values near the tropopause in 2015 are lower than the values observed on 8 August 2009. The variability of water vapour near the tropopause is smaller, with values from 4 ppmv to 18 ppmv. On 10 August, water vapour mixing ratios are as low as 5 ppmv around 380 K. Unfortunately, water vapour mixing ratios on 11 August are not useful after quality control, because the CFH instrument entered a thick cloud ~~.~~ (Fig. 9). Therefore, we only focus on the low ozone and low water vapour values (shaded range) near the tropopause on 10 August 2015.

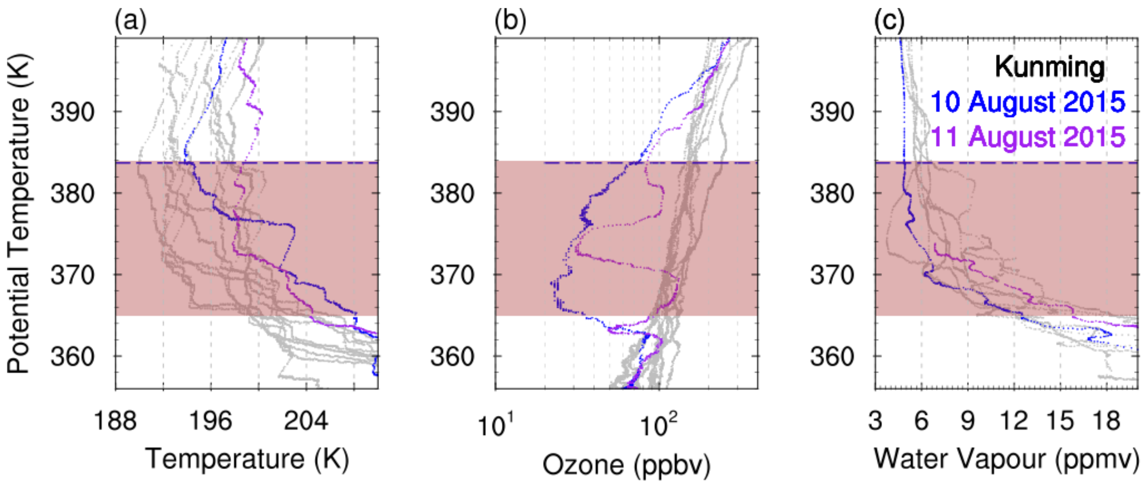

Figure 9. As Fig. 2 but for the case in August 2015.

3.2.1 Background meteorology

Figure 10 shows the 6-day average (5–10 August 2015) of the geopotential height isolines (>16.7 km) at 100 hPa with the temperature, horizontal wind vector, and the tracks of typhoon Soudelor. Typhoon Soudelor formed as a depression on 29 July 2015 over the middle of the Pacific. It became strong during the period of 3–8 August with reaching peak intensity on 3 August as a Category 5 on the Saffir-Simposon hurricane wind scale. On 9 August 2015, Soudelor degraded to a tropical depression. Soudelor was the most intense tropical cyclone of the 2015 Pacific typhoon season. The tracks of typhoon Soudelor are just right below the southeast edge of the ASM anticyclone during the period of 6–10 August. ~~This dynamical condition creates~~ These circumstances create favorable conditions for air parcels on top of the typhoon to be transported into the southern flank of the ASM anticyclonic circulation.

3.2.2 Low ozone in the tropopause layer

Figure 11a shows the mean ozone profile in the rectangle region bounded by purple line in Fig. 10 measured on 31 July, 2, 4, 6, 8, and 10 August ~~from~~ by MLS. On 31 July and 2 August, the rectangle region was without any influence of typhoon Soudelor. Ozone profiles from MLS show that the ozone concentration near the tropopause is approximately 50 ppbv ~~on~~ at 350 K. In contrast, MLS measurements show that the ozone concentration in the upper troposphere (352–370 K) is about 20 ppbv during

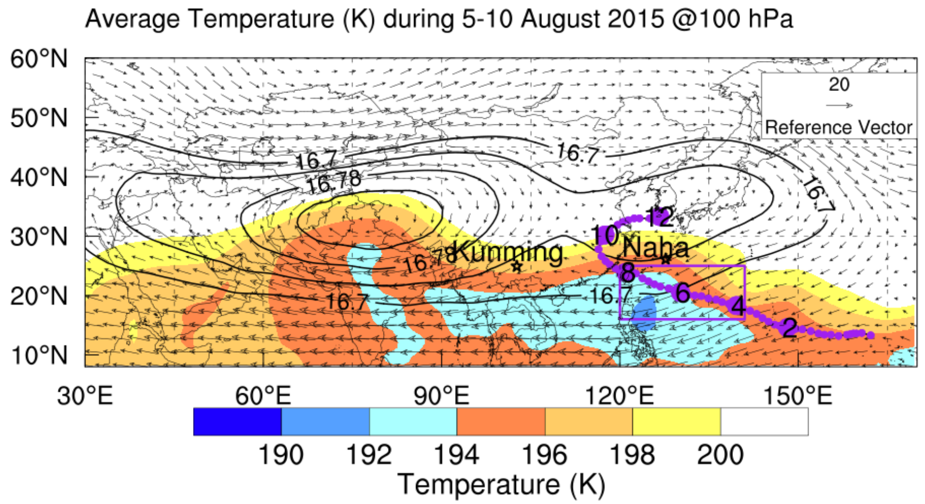

Figure 10. As Fig. 3 but for the case in August 2015 and typhoon Soudelor.

the passage of typhoon Soudelor on 4, 6, and 8 August. Ozone values quickly return to a normal value (∼50 ppbv) during the post-typhoon period on 10 August.

A balloon was launched at Naha site, Japan on 5 August 2015 before typhoon Soudelor passed through. As Fig. 11b shows, low ozone values (22 ppbv) appeared between 352 K and 368 K. This further confirms that deep convection associated with the typhoon Soudelor can uplift air parcels from the boundary layer with low ozone to the tropopause layer. Balloon measurements on 10 August over Kunming captured extremely low ozone between ∼363–382 K (∼14.5–17.5 km) with mixing ratios around 22 ppbv as shown in Figure 11c. The ozone and water vapour at 363–382 K are lower by 80% and 20% compared to the monthly mean value, respectively (Fig. A5). Temperatures and ozone from the ERA-Interim and ERA5 reanalysis data were interpolated to the balloon ascent profile. The temperatures from ERA-Interim, ERA5, and from the radiosonde agree very well in the free troposphere and in the lower stratosphere. However, the temperatures from ERA-Interim and ERA5 differ from the radiosonde measurements at the tropopause. The ERA5 ozone profile is in better agreement with ozonesonde measurements in Kunming, especially in the tropopause region, compared to ERA-Interim in August 2015.

A comparison of diabatic and kinematic trajectory calculations is shown based on ERA-Interim and ERA5 reanalysis in Fig. 12. Air parcels from the western Pacific, merged in the easterly wind flow at the southern flank of the ASM anticyclone, via Naha, Ishigakijima, Laoag, Shantou, Hongkong, Wuzhou, and Haikou, and then were transported to Kunming within 5 days (Figs. 12a–d). Both the kinematic and diabatic trajectories from the ERA-Interim and ERA5 reanalysis data show the lowest temperature region (<190 K) over southern China during the period 7–9 August. Only the ERA5-kinematic ~~trajectory shows~~ trajectories show the typical spiral structure of tropical cyclones (Figs. 12c).

The main difference between the backward trajectories based on ERA-Interim and ERA5 originates from the vertical transport over the western Pacific, where typhoon Soudelor occurred (Figs. 12e–h). Although all of the backward trajectory calculations show vertical transport within the deep convection, the timescale and the strength of air parcels' transport are very

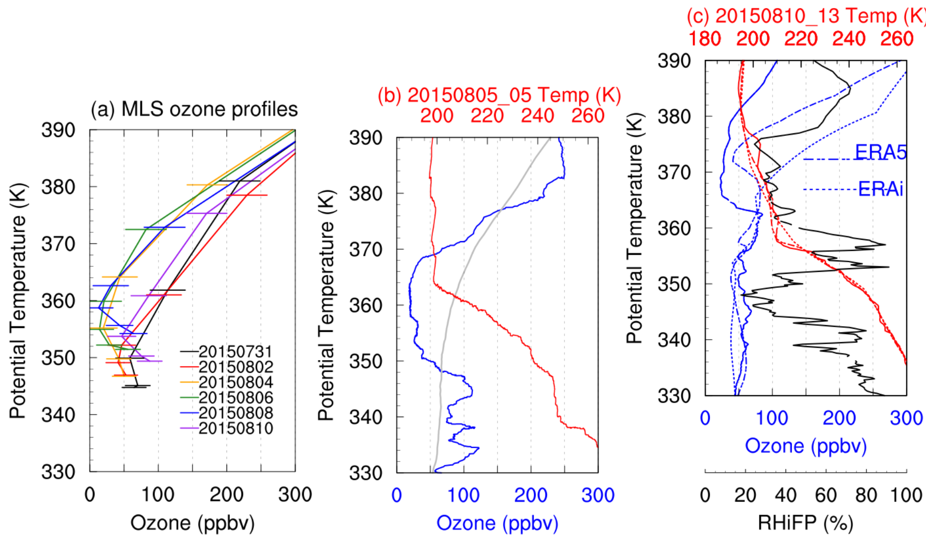

Figure 11. (a) Mean ozone profiles measured from MLS satellite data before, during, and after Soudelor pass through the purple rectangle region of Fig. 10. Profiles of ozone (blue), mean ozone (grey), ~~RH~~ RHFP (~~θ~~ black), and temperature (red) in (b) Naha and (c) Kunming. Solid line–observation, dashed line–ERA-interim, dash-dotted line–ERA5.

different. The timescale for the vertical transport from the lower troposphere to the tropopause layer is about 4 days (1–4 August) based on ERA-Interim kinematic and diabatic trajectories. ~~While~~ In contrast the timescale is 2 days (6–7 August) based on the ERA5 kinematic and diabatic trajectories. Both the kinematic and diabatic trajectories from ERA5 show faster vertical transport than ERA-Interim backward trajectories. The time series of the lowest temperature from Haikou, Wuzhou, Hong Kong, Shantou, Laoag, and Ishigakijima are shown based on upper air soundings (Fig. 13). Balloon measurements in Haikou captured the lowest temperature (187 K) during 7–8 August 2015 near the tropopause. Upper air soundings from Ishigakijima, Laoag, Shantou, Hongkong, and Wuzhou also show the lowest temperature tropopause layer (190–194 K) during 6–10 August 2015.

3.2.3 Dehydration based on the ERA-Interim and ERA5 reanalysis data

Figure 14 displays the ~~cloud top temperature (CTT)~~ brightness temperature from FY-2G satellite with air parcels' locations at the corresponding time based on ERA-Interim diabatic trajectory calculations and ERA5 kinematic and diabatic trajectories. On 5 August, Naha was located at the ~~northwestern~~ northern edge of typhoon Soudelor (Fig. 14a). A balloon launched at Naha captured the low ozone mixing ratios in the TTL as Fig. 11b shows. On 6 August, air parcels from ERA5 kinematic and diabatic trajectory calculations were located above the center of Soudelor (Fig. 14b). Some of the air parcels from the ERA-Interim diabatic trajectory calculations still were located at the edge of typhoon Soudelor. Air parcels moved westward toward Kunming on 8 August (Fig. 14c), and ~~CTT show the lowest temperature (~~ the lowest brightness temperature is 190 K ~~)~~ above Taiwan. On 9 August, air parcels arrived in Kunming under clear sky conditions (Fig. 14d).

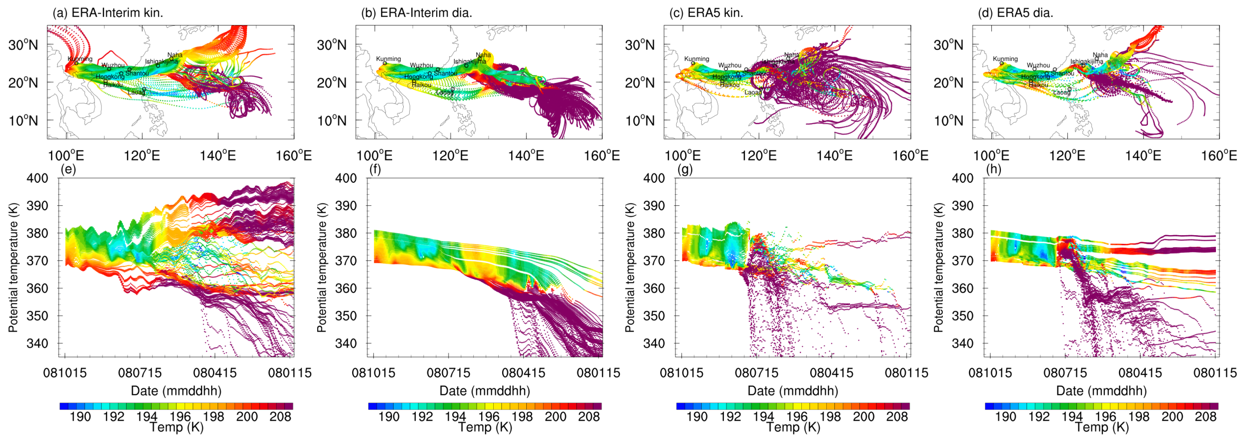

Figure 12. As Fig. 5 but for the case on 10 August 2015.

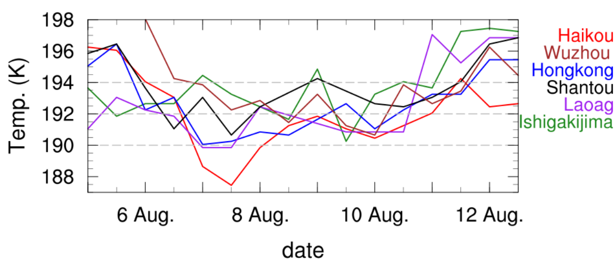

Figure 13. As Fig. 6 but for the case in 2015.

Figures 15a and b show the temperature along the 4-day backward trajectories for air parcels at ~~370–381~~374–381 K on 10 August 2015 with ~~CTT~~ the brightness temperature from FY-2G. From 00:00 UTC on 7 August to 12:00 UTC on 8 August, the air parcels are located at the top of the deep convection associated with typhoon Soudelor according to the ~~CTT of~~ FY-2G brightness temperature (Figs. 15a and b). Before air parcels enter the lowest temperature region, the water vapour mixing ratios from the MLS satellite are 7 ± 0.3 ppmv at 05:30 UTC on 8 August at 100 hPa (Figs. 15c and d). Two days later, the water vapour mixing ratios observed by CFH are approximately 5 ppmv in Kunming (red dot on right-hand side of Fig. 15), hence have significantly decreased after the air parcels passed through the lowest temperature region from 05:00 UTC to 21:00 UTC on 8 August 2015. The $\mathrm{RH_i}$ is calculated ~~according to~~ from the observed water vapour mixing ratios (CFH ~~observed~~ on 10 August) divided by the SMR (Figs. 15e and f). Air parcels experienced supersaturation during the lowest temperature period based on ERA5 diabatic trajectory calculations. Freezing and drying processes contribute to the variability of water vapour mixing ratios observed over Kunming in August 2015 again ~~.~~ as for the case in 2009.

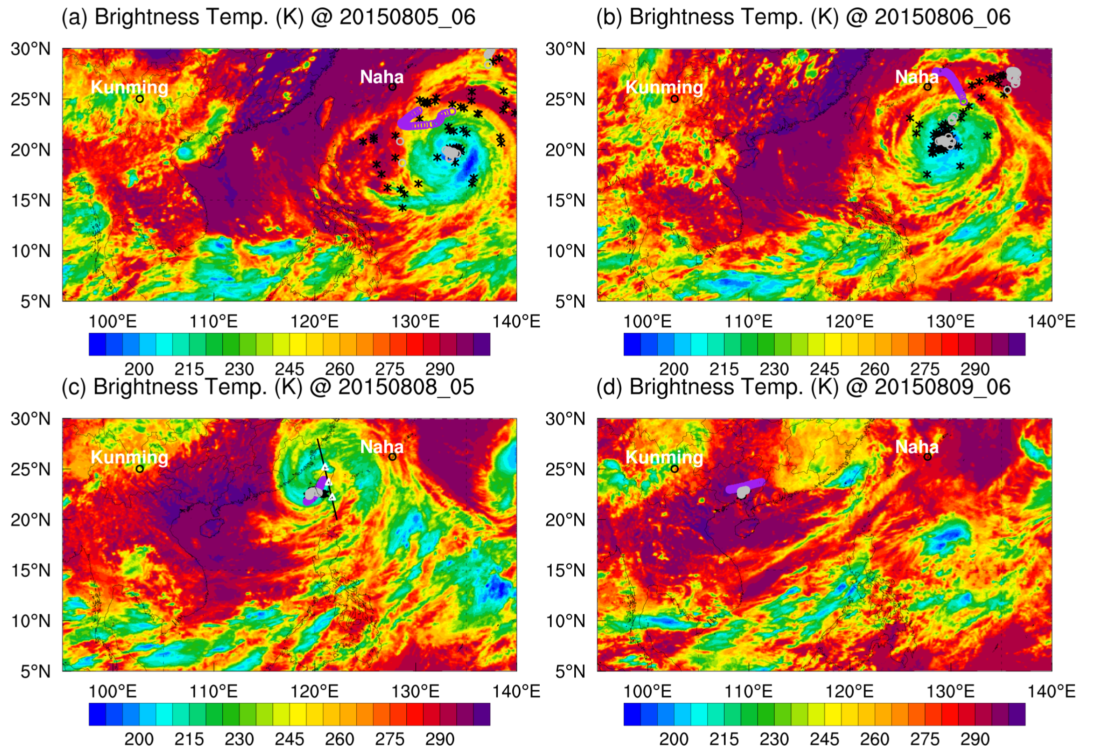

Figure 14. ~~Cloud top~~ Brightness temperature from FY-2G satellite on (a) 5 August, (b) 6 August, (c) 8 August, and (d) 9 August 2015 with backward trajectories (grey circles–ERA5 diabatic, black asterisk–ERA5 diabatic, purple circles–ERA-Interim diabatic) for air parcels with low ozone and low water vapour.

4 Discussion and conclusions

The low ozone and low water vapour mixing ratios near the tropopause measured on 8 August 2009 and 10 August 2015 in Kunming are investigated using balloon measurements, satellite measurements, and CLaMS simulations. MLS ozone and water vapour measurements and trajectory calculations from the CLaMS model confirm that the vertical (horizontal) transport is largely caused by tropical cyclones~~and~~ , whereas the horizontal transport is caused by the ASM anticyclone. The interplay between tropical cyclones and the ASM anticyclone exerts a major influence on transporting the ozone-poor western Pacific boundary air to the tropopause layer and even to the ASM anticyclone region. This interplay is consistent with ~~a former~~ an earlier study by Li et al. (2017) analysing low ozone values in Lhasa measured in August 2013. The deep convective clouds associated with tropical cyclones have considerable implications on ozone in the UTLS (Fu et al., 2013; Li et al., 2017) and in consequence other chemical species, such as the hydroxyl radical (Rex et al., 2014).

~~Besides tropical cyclones, other potential mechanisms (wave activity) can also contribute to dehydration in the tropopause layer (Fujiwara et al., 2012).~~ The lowest temperatures at the tropopause over the western Pacific ocean mainly drive the dehydration process. As a result, air parcels become dry when they pass the low temperature region before entering the stratosphere.

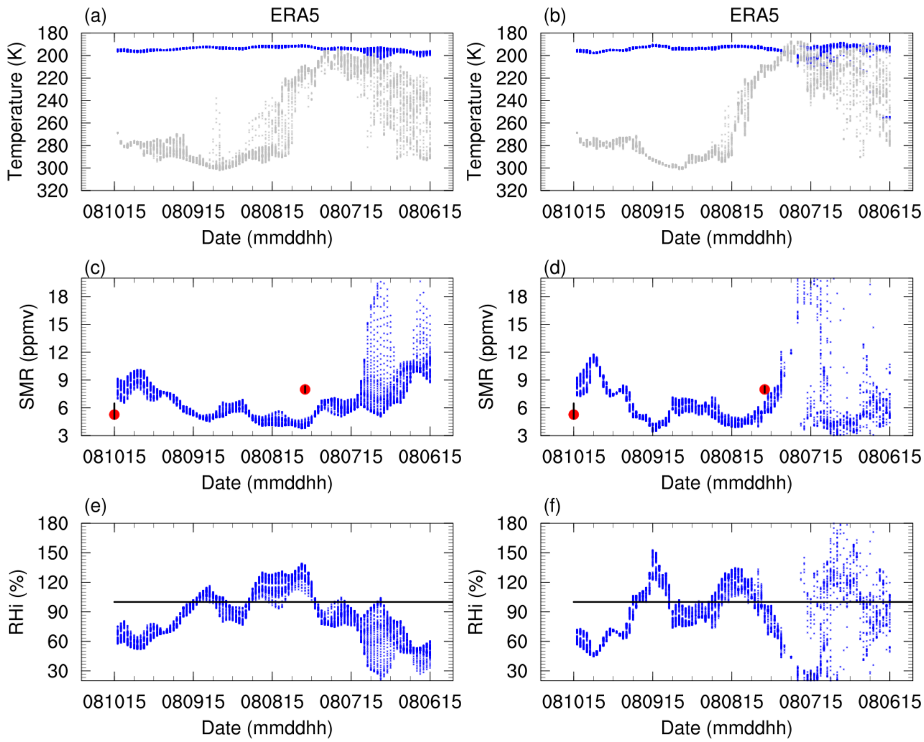

Figure 15. As Fig. 8 but for the case on 10 August 2015.

Holton and Gettelman (2001) ~~call that~~ called this "the cold trap in winter". Our case ~~study for the summer season~~ studies show that the low temperature (<190 K) at the outflow of deep convective clouds associated with tropical cyclones causes freeze-drying in the tropopause layer during the summer season at the southeastern edge of the ASM. This result is consistent with ~~this low temperature picture, with~~ results of Holton and Gettelman (2001) demonstrating that the low temperatures in winter, with the lowest temperatures also occurring over the western Pacific~~and at the southeastern edge of the ASM, however, further north compared to winter condition~~, and causing freeze-drying in the winter tropopause layer. Besides tropical cyclones, other potential mechanisms (wave activity) can also contribute to dehydration in the tropopause layer (Fujiwara et al., 2012).

Our observations further confirm previous studies (Hasebe et al., 2013; Inai et al., 2013; Wright et al., 2011), that air masses emanating from the South China and Philippine Sea become particularly dry when they pass through the lowest temperature regions around the tropopause over the western Pacific. ~~The~~ We found that the easterly winds on the southern flank of the ASM anticyclone transport these air masses with low ozone and low water vapour to the west over a distance of approximately 2,000 km to Kunming.

~~The interplay between tropical cyclones and the ASM anticyclone has the potential to impact the long term trends of ozone, water vapour , and even the optically thin cirrus near the tropopause, particularly under climate change conditions, when the occurrence of tropical cyclones will be more frequently.~~

This observation is different from the features of low ozone and high water vapour in the ASM anticyclone (Park et al., 2007). The trajectory calculations using ERA5 data show faster and stronger vertical transport than those based on ERA-Interim reanalysis data. The ERA5 wind field appears to represent convective updrafts and tropical cyclones ~~well~~much better than ERA-Interim, due to ERA5's better spatial and temporal resolution. This is consistent with the stronger vertical transport in ERA5 compared to ERA-Interim reanalysis data. ERA5 backward trajectories show stronger dispersion of temperature values than ERA-Interim trajectories, by comparing of the ERA-Interim and ERA5 reconstructed $\mathrm{SMR}_{\mathrm{min}}$ with the water vapour mixing ratio observed by CFH (Fig. B1).

The interplay between tropical cyclones and the ASM anticyclone has the potential to impact the long term trends of ozone, water vapour, and even optically thin cirrus near the tropopause, particularly under climate change conditions, when the occurrence of tropical cyclones is expected to increase.

Code and data availability. ERA-Interim and ERA5 meteorological reanalysis data are freely available from the web page: http://apps.ecmwf.int/datasets/ (last access: 3 August 2018). The MLS ozone and water vapour data were downloaded from https://acdisc.gesdisc.eosdis.nasa.gov/data/ (last access: 3 November 2017). The FY-2D and FY-2G data used in this study can be obtained at http://satellite.nsmc.org.cn/PortalSite/Data/Satellite.aspx (last access: 14 June 2018). The ozone profiles for Naha are provided on the World Ozone and Ultraviolet Radiation Data Centre (WOUDC) https://woudc.org/data/explore.php?lang=en (last access: 15 June 2018). The upper air soundings data were downloaded from the University of Wyoming http://weather.uwyo.edu/upperair/sounding.html (last access: 12 September 2018). The SWOP data of this paper are available upon request to Jianchun Bian (bjc@mail.iap.ac.cn). The CLaMS backward trajectories calculations may be requested from Dan Li (lidan@mail.iap.ac.cn). The CLaMS model code can be requested from Dr. Rolf Müller (ro.mueller@fz-juelich.de)

Appendix A: Comparisons of ERA-Interim and ERA5 wind fields

Figure A1 compares the geopotential height and horizontal wind speeds at 150 hPa on 4, 5, and 6 August 2009 between ERA-Interim and ERA5 reanalysis data. The geopotential height from ERA-Interim and ERA5 data shows a similar pattern. The horizontal wind fields also show the same pattern, but the ERA5 wind fields display more small-scale structures.

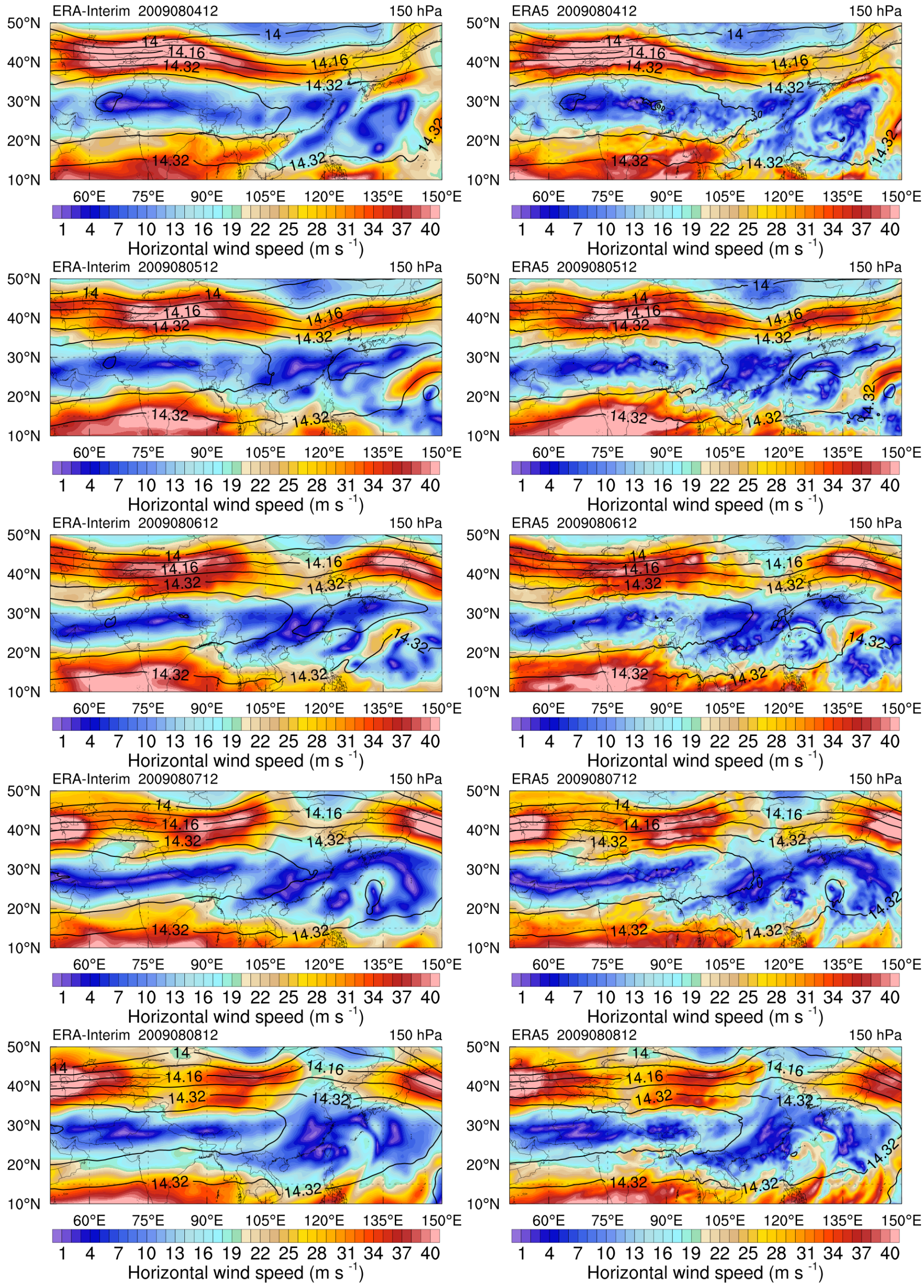

Figure A1. Geopotential height (black lines, gpkm) and horizontal wind speeds (shaded, $\mathrm{m\,s^{-1}}$) at 150 hPa on 4, 5, ~~and~~ 6, 7, and 8 August 2009 from ERA-Interim (left) and ERA5 (right).

Figure A2 shows the relative difference (observation minus monthly mean value divided by monthly mean value) for ozone and water vapour on 8 August 2009. The differences mainly occurred at layers of 364–367 K and 376–384 K with 40%. The ERA-Interim diabatic trajectories for air parcels at 364–367 K is shown in Fig. A3. Air parcels from the western Pacific, moved around the ASM anticyclone, then were transported to Kunming within 10 days. The possible source region and transport pathway for air parcels at 364–367 K are different from air parcels at 376–384 K. The tropical storm Goni transported the air parcels from the marine boundary layer to the tropopause during the period of 30 July and 1 August 2009. Fig. A4 shows the time evolution of the temperature, the saturation water vapour mixing ratio (SMR), relative humidity over ice ($\mathrm{RH_i}$) along 10-day backward trajectories of air parcels on 364–367 K from ERA-Interim diabatic trajectories.

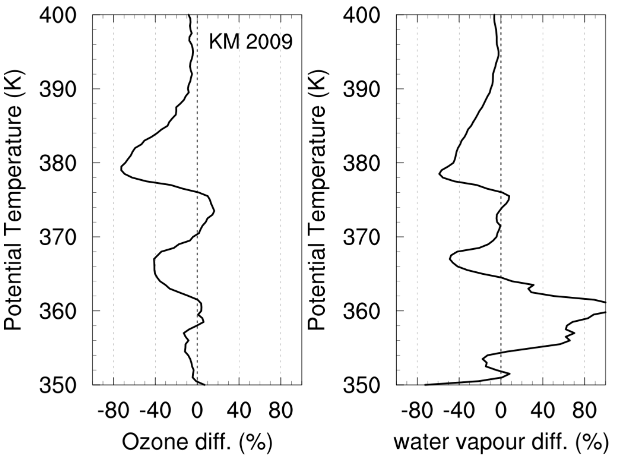

Figure A2. Ozone and water vapour relative difference on 8 August 2009 to the climatologial mean value for August 2009.

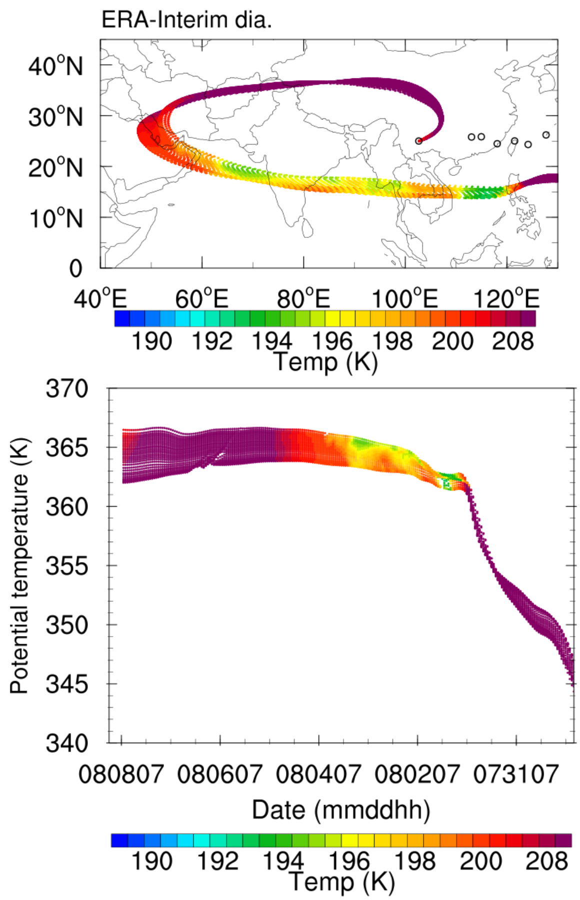

Figure A3. ERA-Interim diabatic trajectories for air parcels started along the measured balloon profile between 364 K and 367 K colour-coded by temperature in (top) longitude–latitude cross section and (bottom) as a function of time vs. potential temperature.

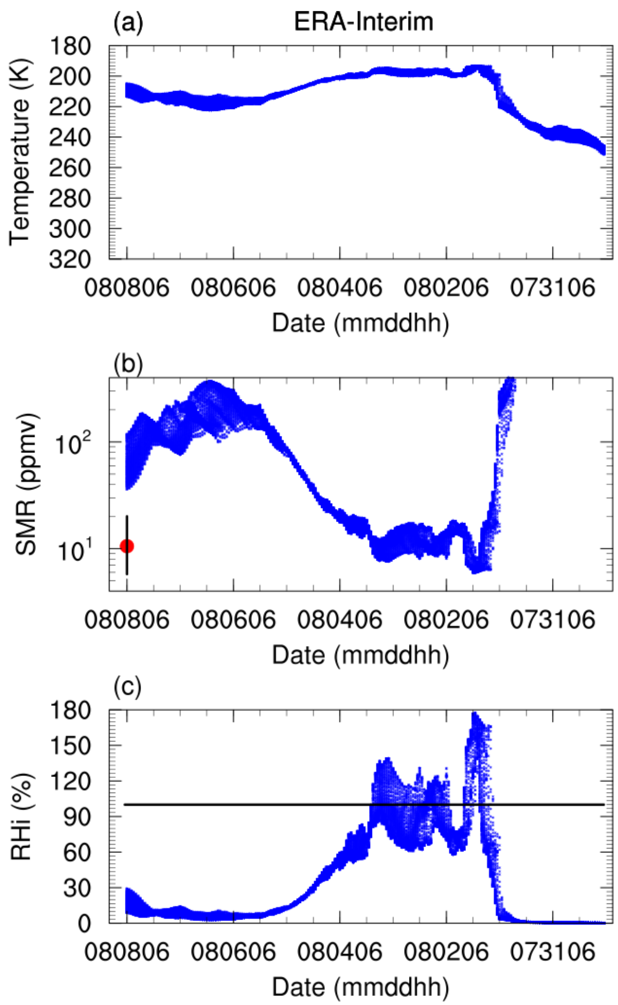

Figure A4. The time evolution of the temperature (blue dots), the saturation water vapour mixing ratio (SMR), relative humidity over ice (RH_i) along 8-day backward trajectories of air parcels on 364–367 K from ERA-Interim diabatic trajectories.

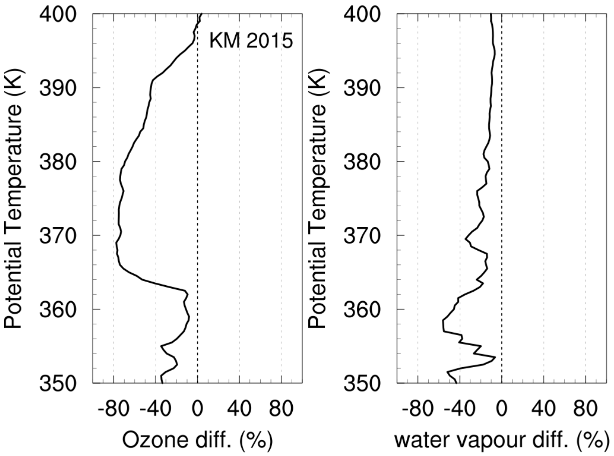

Figure A5. As Fig. A2 but for the case in 2015.

Appendix B: Comparisons of the ERA-Interim and ERA5 reconstructed $\mathrm{SMR_{min}}$ with the water vapour mixing ratio observed by CFH

The authors calculated an ensemble trajectories for nine points around the observation site for cases 1 and 2. The minimum SMR for each trajectory is selected before air parcel met the cloud as Fig. B1 shows. For the 2009 case, the one sigma standard deviation of reconstructed water vapour of the ensemble of backward trajectories in the region of interest (378–384 K) agree well with observations. ERA5 reconstructed water vapour is below observed water vapour, but still in the one sigma standard deviation range. For the 2015 case, for both ERA-Interim and ERA5 the range of reconstructed water vapour is below the observations in the region of interest (376–382 K). However, in the region of interest the variability of reconstructed water vapour of ERA5 ensemble trajectories is much higher than ERA-Interim trajectories. This demonstrates the stronger dispersion of temperature values along ERA5 backward trajectories caused by the high resolution of ERA5 data. In contrast, ERA-Interim trajectories are going through nearly the same cold point temperature yield a much lower variability of reconstructed water vapour.

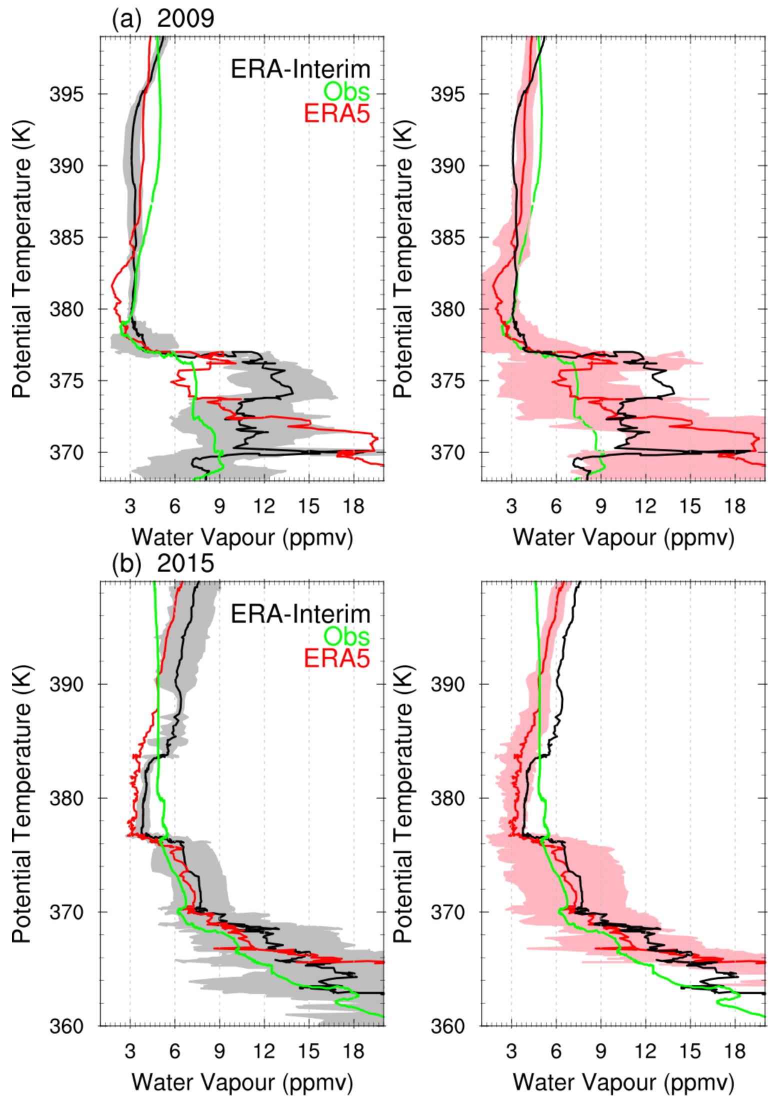

Figure B1. Water vapour profiles (green line) measured by CFH on (a) 8 August 2009 and (b) 10 August 2015 and mean reconstructed water vapour based on diabatic trajectories using ERA-Interim (black line) and ERA5 (red line) for 2009 and 2015. The grey/pink regions show the one sigma standard deviation range of the ensemble of backward trajectories.

Author contributions. DL prepared for the first draft. BV, RM, GG, FP, and MR provided effective and constructive comments and helped improve the paper. JB and HV gave useful comments. JB, ZB, QL, JZ, and DL made the balloon-borne measurements in Kunming. HV supported for the measurements. All coauthors contributed to writing the paper

Competing interests. The authors declare that they have no conflict of interest

Acknowledgements. This research was supported by the National Key Research and Development program of China (2018YFC1505703) and the National Natural Science Foundation of China (Grant No. 91837311, 41975050, 41605025, 41675040, 91637104, and 41705127). Our activities contribute to the European Community's Seventh Framework Programme (FP7/2007-2013) as part of the StratoClim project (Grant agreement No. 603557). The authors thank the Strategic Priority Research Program of Chinese Academy of Sciences (Grant No. XDA17010102), the International Postdoctoral Exchange Fellowship Program 2017 under grant No. 20171015 and China Postdoctoral Science Foundation (2015M581153). Finally, we wish to thank three anonymous reviewers for very constructive suggestions.)

References

Bergman, J. W., Fierli, F., Jensen, E. J., Honomichl, S., and Pan, L. L.: Boundary layer sources for the Asian anticyclone: Regional contributions to a vertical conduit, J. Geophys. Res. Atmos., 118, 2560–2575, https://doi.org/10.1002/jgrd.50142, 2013.

Bian, J. C., Pan, L. L., Paulik, L., Vömel, H., and Chen, H. B.: In situ water vapor and ozone measurements in Lhasa and Kunming during the Asian summer monsoon, Geophys. Res. Lett., 39, L19808, https://doi.org/10.1029/2012GL052996, 2012.

Cairo, F., Buontempo, C., MacKenzie, A. R., Schiller, C., Volk, C. M., Adriani, A., Mitev, V., Matthey, R., Di Donfrancesco, G., Oulanovsky, A., Ravegnani, F., Yushkov, V., Snels, M., Cagnazzo, C., and Stefanutti, L.: Morphology of the tropopause layer and lower stratosphere above a tropical cyclone: a case study on cyclone Davina (1999), Atmos. Chem. Phys., 8, 3411–3426, https://doi.org/10.5194/acp-8-3411-2008, 2008.

Chen, B., Xu, X. D., Yang, S., and Zhao, T. L.: Climatological perspectives of air transport from atmospheric boundary layer to tropopause layer over Asian monsoon regions during boreal summer inferred from Lagrangian approach, Atmos. Chem. Phys., 12, 5827–5839, https://doi.org/10.5194/acp-12-5827-2012, 2012.

Dee, D. P., Uppala, S. M., Simmons, A. J., Berrisford, P., Poli, P., Kobayashi, S., Andrae, U., Balmaseda, M. A., Balsamo, G., Bauer, P., Bechtold, P., Beljaars, A. C. M., van de Berg, L., Bidlot, J., Bormann, N., Delsol, C., Dragani, R., Fuentes, M., Geer, A. J., Haimberger, L., Healy, S. B., Hersbach, H., Hólm, E. V., Isaksen, L., Kållberg, P., Köhler, M., Matricardi, M., McNally, A. P., Monge-Sanz, B. M., Morcrette, J.-J., Park, B.-K., Peubey, C., de Rosnay, P., Tavolato, C., Thépaut, J.-N., and Vitart, F.: The ERA-Interim reanalysis: configuration and performance of the data assimilation system, Q. J. R. Meteorol. Soc., 137, 553–597, https://doi.org/10.1002/qj.828, 2011.

Fu, Y. F., Xian, T., Lü, D. R., Liu, G. S., Heng, Z. W., Sun, L., Liu, Q., Wang, Y., and Yang, Y. J.: Ozone vertical variations during a typhoon derived from the OMI observations and reanalysis data, Chin. Sci. Bull., 58, 3890–3894, https://doi.org/10.1007/s11434-013-6024-7, 2013.

Fueglistaler, S., Legras, B., Beljaars, A., Morcrette, J.-J., Simmons, A., Tompkins, A. M., and Uppapla, S.: The diabatic heat budget of the upper troposphere and lower/mid stratosphere in ECMWF reanalyses, Q. J. R. Meteorol. Soc., 135, 638, https://doi.org/10.1002/qj.361, 2009.

Fujiwara, M., Suzuki, J., Gettelman, A., Hegglin, M. I., Akiyoshi, H., and Shibata, K.: Wave activity in the tropical tropopause layer in seven reanalysis and four chemistry climate model data sets, J. Geophys. Res. Atmos., 117, D12105, https://doi.org/10.1029/2011JD016808, 2012.

Garny, H. and Randel, W. J.: Transport pathways from the Asian monsoon anticyclone to the stratosphere, Atmos. Chem. Phys., 16, 2703–2718, https://doi.org/10.5194/acp-16-2703-2016, 2016.

Goff, J. A. and Gratch, S.: Low-pressure properties of water from −160 to 212 F, Trans. Am. Soc. Heating Air-Cond. Eng., 52, 95–122, 1946.

Hasebe, F., Fujiwara, M., Nishi, N., Shiotani, M., Vömel, H., Oltmans, S., Takashima, H., Saraspriya, S., Komala, N., and Inai, Y.: In situ observations of dehydrated air parcels advected horizontally in the Tropical Tropopause Layer of the western Pacific, Atmos. Chem. Phys., 7, 803–813, https://doi.org/10.5194/acp-7-803-2007, 2007.

Hasebe, F., Inai, Y., Shiotani, M., Fujiwara, M., Vömel, H., Nishi, N., Ogino, S.-Y., Shibata, T., Iwasaki, S., Komala, N., Peter, T., and Oltmans, S. J.: Cold trap dehydration in the Tropical Tropopause Layer characterised by SOWER chilled-mirror hygrometer network data in the Tropical Pacific, Atmos. Chem. Phys., 13, 4393–4411, https://doi.org/10.5194/acp-13-4393-2013, 2013.

Hersbach, H. and Dee, D.: ERA5 reanalysis is in production, ECMWF Newsletter, 147, p.7, available at: https://www.ecmwf.int/en/newsletter/147/news/era5-reanalysis-production, 2016.

Hoffmann, L., Günther, G., Li, D., Stein, O., Wu, X., Griessbach, S., Heng, Y., Konopka, P., Müller, R., Vogel, B., and Wright, J. S.: From ERA-Interim to ERA5: the considerable impact of ECMWF's next-generation reanalysis on Lagrangian transport simulations, Atmos. Chem. Phys., 19, 3097–3124, https://doi.org/10.5194/acp-19-3097-2019, 2019.

Holton, J. R. and Gettelman, A.: Horizontal transport and the dehydration of the stratosphere, Geophys. Res. Lett., 28, 2799–2802, 2001.

Höpfner, M., Ungermann, J., Borrmann, S., Wagner, R., Spang, R., Riese, M., Stiller, G., Appel, O., Batenburg, A. M., Bucci, S., Cairo, F., Dragoneas, A., Friedl-Vallon, F., Hünig, A., Johansson, S., Krasauskas, L., Legras, B., Leisner, T., Mahnke, C., Möhler, O., Molleker, S., Müller, R., Neubert, T., Orphal, J., Preusse, P., Rex, M., Saathoff, H., Stroh, F., Weigel, R., and Wohltmann, I.: Ammonium nitrate particles formed in upper troposphere from ground ammonia sources during Asian monsoons, Nat. Geosci., 12, 608–612, https://doi.org/10.1038/s41561-019-0385-8, 2019.

Hyland, R. W. and Wexler, A.: Formulations for the thermodynamic properties of the saturated phases of H_2O from 173.15 K to 473.15 K, ASHRAE Trans., 89, 500–519, 1983.

Inai, Y., Hasebe, F., Fujiwara, M., Shiotani, M., Nishi, N., Ogino, S.-Y., Vömel, H., Iwasaki, S., and Shibata, T.: Dehydration in the tropical tropopause layer estimated from the water vapor match, Atmos. Chem. Phys., 13, 8623–8642, https://doi.org/10.5194/acp-13-8623-2013, 2013.

Komhyr, W. D., Barnes, R. A., Brothers, G. B., Lathrop, J. A., and Opperman, D. P.: Electrochemical concentration cell ozonesonde performance evaluation during STOIC 1989, J. Geophys. Res., 100, 9231–9244, https://doi.org/10.1029/94JD02175, 1995.

Konopka, P., Steinhorst, H.-M., Grooß, J.-U., Günther, G., Müller, R., Elkins, J. W., Jost, H.-J., Richard, E., Schmidt, U., Toon, G., and McKenna, D. S.: Mixing and Ozone Loss in the 1999-2000 Arctic Vortex: Simulations with the 3-dimensional Chemical Lagrangian Model of the Stratosphere (CLaMS), J. Geophys. Res., 109, D02315, https://doi.org/10.1029/2003JD003792, 2004.

Li, D., Vogel, B., Bian, J., Müller, R., Pan, L. L., Günther, G., Bai, Z., Li, Q., Zhang, J., Fan, Q., and Vömel, H.: Impact of typhoons on the composition of the upper troposphere within the Asian summer monsoon anticyclone: the SWOP campaign in Lhasa 2013, Atmos. Chem. Phys., 17, 4657–4672, https://doi.org/10.5194/acp-17-4657-2017, 2017.

Li, D., Vogel, B., Müller, R., Bian, J., Günther, G., Li, Q., Zhang, J., Bai, Z., Vömel, H., and Riese, M.: High tropospheric ozone in Lhasa within the Asian summer monsoon anticyclone in 2013: influence of convective transport and stratospheric intrusions, Atmos. Chem. Phys., 18, 17 979–17 994, https://doi.org/10.5194/acp-18-17979-2018, 2018.

Livesey, N. J., Read, W. G., Wagner, P. A., Froidevaux, L., Lambert, A., Manney, G. L., Millán Valle, L. F., Pumphrey, H. C., Santee, M. L., Schwartz, M. J., Wang, S., Fuller, R. A., Jarnot, R. F., Knosp, B. W., Martinez, E., and Lay, R. R.: Version 4.2x Level 2 data quality and description document, JPL D-33509 Rev. D, https://mls.jpl.nasa.gov/data/v4-2_data_quality_document.pdf, 2018.

McKenna, D. S., Konopka, P., Grooß, J.-U., Günther, G., Müller, R., Spang, R., Offermann, D., and Orsolini, Y.: A new Chemical Lagrangian Model of the Stratosphere (CLaMS): 1. Formulation of advection and mixing, J. Geophys. Res., 107, 4309, https://doi.org/10.1029/2000JD000114, 2002.

Minschwaner, K., Manney, G. L., Petropavlovskikh, I., Torres, L. A., Lawrence, Z. D., Sutherland, B., Thompson, A. M., Johnson, B. J., Butterfield, Z., Dubey, M. K., Froidevaux, L., Lambert, A., Read, W. G., and Schwartz, M. J.: Signature of a tropical Pacific cyclone in the composition of the upper troposphere over Socorro, NM, Geophys. Res. Lett., 42, 9530–9537, https://doi.org/10.1002/2015GL065824, 2015.

Murphy, D. M. and Koop, T.: Review of the vapour pressures of ice and supercooled water for atmospheric applications, Q. J. R. Meteorol. Soc., 131, 1539–1565, 2005.

Naja, M. and Akimoto, H.: Contribution of regional pollution and long-range transport to the Asia-Pacific region: Analysis of long-term ozonesonde data over Japan, J. Geophys. Res., 109, https://doi.org/10.1029/2004JD004687, 2004.

Newton, R., Vaughan, G., Hintsa, E., Filus, M. T., Pan, L. L., Honomichl, S., Atlas, E., Andrews, S. J., and Carpenter, L. J.: Observations of ozone-poor air in the tropical tropopause layer, Atmos. Chem. Phys., 18, 5157–5171, https://doi.org/10.5194/acp-18-5157-2018, 2018.

Pan, L. L., Honomichl, S. B., Kinnison, D. E., Abalos, M., Randel, W. J., Bergman, J. W., and Bian, J. C.: Transport of chemical tracers from the boundary layer to stratosphere associated with the dynamics of the Asian summer monsoon, J. Geophys. Res. Atmos., 121, 14,159–14,174, https://doi.org/10.1002/2016JD025616, 2016.

Park, M., Randel, W. J., Gettleman, A., Massie, S. T., and Jiang, J. H.: Transport above the Asian summer monsoon anticyclone inferred from Aura Microwave Limb Sounder tracers, J. Geophys. Res., 112, D16309, https://doi.org/10.1029/2006JD008294, 2007.

Park, M., Randel, W. J., Emmons, L. K., Bernath, P. F., Walker, K. A., and Boone, C. D.: Chemical isolation in the Asian monsoon anticyclone observed in Atmospheric Chemistry Experiment (ACE-FTS) data, Atmos. Chem. Phys., 8, 757–764, https://doi.org/10.5194/acp-8-757-2008, 2008.

Ploeger, F., Konopka, P., Günther, G., Grooß, J.-U., and Müller, R.: Impact of the vertical velocity scheme on modeling transport across the tropical tropopause layer, J. Geophys. Res., 115, D03301, https://doi.org/10.1029/2009JD012023, 2010.

Ploeger, F., Fueglistaler, S., Grooß, J.-U., Günther, G., Konopka, P., Liu, Y. S., Müller, R., Ravegnani, F., Schiller, C., Ulanovski, A., and Riese, M.: Insight from ozone and water vapour on transport in the tropical tropopause layer (TTL), Atmos. Chem. Phys., 11, 407–419, https://doi.org/10.5194/acp-11-407-2011, 2011.

Pommrich, R., Müller, R., Grooß, J.-U., Konopka, P., Ploeger, F., Vogel, B., Tao, M., Hoppe, C. M., Günther, G., Spelten, N., Hoffmann, L., Pumphrey, H.-C., Viciani, S., D'Amato, F., Volk, C. M., Hoor, P., Schlager, H., and Riese, M.: Tropical troposphere to stratosphere transport of carbon monoxide and long-lived trace species in the Chemical Lagrangian Model of the Stratosphere (CLaMS), Geosci. Model Dev., 7, 2895–2916, https://doi.org/10.5194/gmd-7-2895-2014, 2014.

Randel, W. J., Park, M., Emmons, L., Kinnison, D., Bernath, P., Walker, K. A., Boone, C., and Pumphrey, H.: Asian Monsoon Transport of Pollution to the Stratosphere, Science, 328, 611–613, https://doi.org/10.1126/science.1182274, 2010.

Randel, W. J., Zhang, K., and Fu, R.: What controls stratospheric water vapor in the NH summer monsoon regions?, J. Geophys. Res. Atmos., 120, 7988–8001, https://doi.org/10.1002/2015JD023622, 2015.

Read, K. A., Mahajan, A. S., Carpenter, L. J., Evans, M. J., Faria, B. V. E., Heard, D. E., Hopkins, J. R., Lee, J. D., Moller, S. J., Lewis, A. C., Mendes, L., McQuaid, J. B., Oetjen, H., Saiz-Lopez, A., Pilling, M. J., and Plane, J. M. C.: Extensive halogen-mediated ozone destruction over the tropical Atlantic Ocean, Nature, 453, 1232–1235, https://doi.org/10.1038/nature07035, 2008a.

Read, W. G., Schwarz, M. J., Lambert, A., Su, H., Livesey, N.-J., Daffer, W. H., and Boone, C. D.: The roles of convection, extratropical mixing and in-situ freeze-drying in the Tropical Tropopause Layer, Atmos. Chem. Phys., 8, 6051–6067, https://doi.org/10.5194/acp-8-6051-2008, 2008b.

Rex, M., Wohltmann, I., Ridder, T., Lehmann, R., Rosenlof, K., Wennberg, P., Weisenstein, D., Notholt, J., Krüger, K., Mohr, V., and Tegtmeier, S.: A tropical West Pacific OH minimum and implications for stratospheric composition, Atmos. Chem. Phys., 14, 4827–4841, https://doi.org/10.5194/acp-14-4827-2014, 2014.

Schiller, C., Grooß, J.-U., Konopka, P., Plöger, F., Silva dos Santos, F. H., and Spelten, N.: Hydration and dehydration at the tropical tropopause, Atmos. Chem. Phys., 9, 9647–9660, https://doi.org/10.5194/acp-9-9647-2009, 2009.

Schoeberl, M. R. and Dessler, A. E.: Dehydration of the stratosphere, Atmos. Chem. Phys., 11, 8433–8446, https://doi.org/10.5194/acp-11-8433-2011, 2011.

Schoeberl, M. R., Douglass, A. R., Zhu, Z. X., and Pawson, S.: A comparison of the lower stratospheric age spectra derived from a general circulation model and two data assimilation systems, J. Geophys. Res., 108, 4113, https://doi.org/10.1029/2002JD002652, 2003.

Shi, C. H., Zhang, C. X., and Guo, D.: Comparison of electrochemical concentration cell ozonesonde and microwave limb sounder satellite remote sensing ozone profiles for the center of the South Asian High, Rem. Sens., 9, https://doi.org/10.3390/rs9101012, 2017.

Tissier, A.-S. and Legras, B.: Convective sources of trajectories traversing the tropical tropopaus layer, Atmos. Chem. Phys., 16, 3383–3398, https://doi.org/10.5194/acp-16-3383-2016, 2016.

Vogel, B., Günther, G., Müller, R., Grooß, J.-U., Hoor, P., Krämer, M., Müller, S., Zahn, A., and Riese, M.: Fast transport from Southeast Asia boundary layer sources to northern Europe: rapid uplift in typhoons and eastward eddy shedding of the Asian monsoon anticyclone, Atmos. Chem. Phys., 14, 12 745–12 762, https://doi.org/10.5194/acp-14-12745-2014, 2014.

Vogel, B., Günther, G., Müller, R., Grooß, J.-U., and Riese, M.: Impact of different Asian source regions on the composition of the Asian monsoon anticyclone and of the extratropical lowermost stratosphere, Atmos. Chem. Phys., 15, 13 699–13 716, https://doi.org/10.5194/acp-15-13699-2015, 2015.

Vogel, B., Müller, R., Günther, G., Spang, R., Hanumanthu, S., Li, D., Riese, M., and Stiller, G. P.: Lagrangian simulations of the transport of young air masses to the top of the Asian monsoon anticyclone and into the tropical pipe, Atmos. Chem. Phys., 19, 6007–6034, https://doi.org/10.5194/acp-2018-724, 2019.

Vömel, H., Naebert, T., Dirksen, R., and Sommer, M.: An update on the uncertainties of water vapor measurements using cryogenic frost point hygrometers, Atmos. Meas. Tech., 9, 3755–3768, https://doi.org/10.5194/amt-9-3755-2016, 2016.

Vömel, H., David, D. E., and Smith, K.: Accuracy of tropospheric and stratospheric water vapor measurements by the cryogenic frost point hygrometer: Instrumental details and observations, J. Geophys. Res., 112, D08305, https://doi.org/10.1029/2006JD007224, 2007.

von Glasow, R., Sander, R., Bott, A., and Crutzen, P. J.: Modeling halogen chemistry in the marine boundary layer 1. Cloud-free MBL, J. Geophys. Res., 107, 4341, https://doi.org/10.1029/2001JD000942, 2002.

WMO: Definition of the tropopause, WMO Bull, IV (4),, pp. 134–138, 1957.

Wright, J. S., Fu, R., Fueglistaler, S., Liu, Y. S., and Zhang, Y.: The influence of summertime convection over Southeast Asia on water vapor in the tropical stratosphere, J. Geophys. Res., 116, D12302, https://doi.org/10.1029/2010JD015416, 2011.

Yan, R. C. and Bian, J. C.: Tracing the boundary layer sources of carbon monoxide in the Asian summer monsoon anticyclone using WRF–Chem, Adv. Atmos. Sci., 32, 943–951, https://doi.org/10.1007/s00376-014-4130-3, 2015.